Geophysical Journal International

Geophys. J. Int. (2010) **182,** 203–232 doi: 10.1111/j.1365-246X.2010.04619.x

Revised Pacific M-anomaly geomagnetic polarity timescale

Masako Tominaga* and William W. Sager

Department of Oceanography, Texas A&M University, 3146 *TAMU College Station,* TX 77843-3146*, USA. E-mail: mtominaga@whoi.edu*

Accepted 2010 April 8. Received 2010 March 16; in original form 2008 September 30

SUMMARY

The current M-anomaly geomagnetic polarity timescale (GPTS) is mainly based on the Hawaiian magnetic lineations in the Pacific Ocean. M-anomaly GPTS studies to date have relied on a small number of magnetic profiles, a situation that is not ideal because any one profile contains an uncertain amount of geologic 'noise' that perturbs the magnetic field signal. Compiling a polarity sequence from a larger array of magnetic profiles is desirable to provide greater consistency and repeatability. We present a new compilation of the M-anomaly GPTS constructed from polarity models derived from magnetic profiles crossing the three lineation sets (Hawaiian, Japanese and Phoenix) in the western Pacific. Polarity reversal boundary locations were estimated with a combination of inverse and forward modelling of the magnetic profiles. Separate GPTS were established for each of the three Pacific lineation sets, to allow examination of variability among the different lineation sets, and these were also combined to give a composite timescale. Owing to a paucity of reliable direct dates of the M-anomalies on ocean crust, the composite model was time calibrated with only two ages; one at each end of the sequence. These two dates are 125.0 Ma for the base of M0r and 155.7 Ma for the base of M26r. Relative polarity block widths from the three lineation sets are similar, indicating a consistent Pacific-wide spreading regime. The new GPTS model shows slightly different spacings of polarity blocks, as compared with previous GPTS, with less variation in block width. It appears that the greater polarity chron irregularity in older models is mostly an artifact of modelling a small number of magnetic profiles. The greater averaging of polarity chron boundaries in our model gives a GPTS that is statistically more robust than prior GPTS models and a superior foundation for Late Jurassic–Early Cretaceous geomagnetic and chronologic studies.

Key words: Magnetic anomalies: modelling and interpretation; Reversals: process, time scale, magnetostratigraphy; Marine magnetics and palaeomagnetics.

1 INTRODUCTION

Marine magnetic anomalies are the foundation of the geomagnetic polarity timescale (GPTS) because they provide a nearly continuous record of polarity intervals in time. Indeed, the continuity and repeatability of marine magnetic profiles were a key factor in the acceptance of the theory of seafloor spreading, which linked these anomalies to the process of oceanic crust formation and geologic time (Vine & Matthews 1963). The underlying model is simple, yet it has proved effective for GPTS development: changes in geomagnetic polarity are globally synchronous and the magnetization of the oceanic crust is mainly recorded within a thin layer of uppermost oceanic crust and was acquired at any given time within a narrow region close to the ridge axis. With these assumptions, early GPTS models were formulated (Heirtzler *et al.* 1968; Larson & Pitman 1972) and subsequently improved by the analyses of greater numbers of magnetic profiles or the acquisition of better age constraints (e.g. Cande & Kent 1992a; Channell *et al.* 1995). Seafloor spreading anomaly polarity block models can often be tied to land magnetostratigraphy and geochronology to obtain polarity boundary ages (Cande & Kent 1992a).

Current GPTS models based on seafloor spreading cover the period from present to Middle Jurassic (Cande & Kent 1992a; Channell *et al.* 1995; Gradstein *et al.* 2005). The marine magnetic anomalies are grouped into two sequences: one before and the other after the Cretaceous Normal Superchron. Anomalies of the Late Cretaceous- Cenozoic Mixed Polarity Superchron (i.e. 'C-anomalies') stretch from Late Cretaceous to present whereas those of the Jurassic-Cretaceous Mixed Polarity Superchron (i.e. 'M-anomalies') span from Middle Jurassic to Early Cretaceous. The currently accepted C-anomaly GPTS was constructed from magnetic profiles from the South Atlantic Ocean and a few profiles from other oceans (Cande & Kent 1992a, 1995). This GPTS is widely accepted because it was constructed from a large number ($n = 5$–9) of carefully selected magnetic profiles, it accounted for

*Now at: Woods Hole Oceanographic Institution.

anomaly skewness (asymmetry) owing to paleolatitude and strike (Schouten & McCamy 1972; Schouten & Cande 1976; Petronotis *et al.* 1992), and its age calibration is derived from a relatively large number ($n = 9$) of radiometric dates.

In contrast, current M-anomaly GPTS are not as well defined because they are based on a smaller number of magnetic profiles, and are primarily focused on the Hawaiian lineation set in the western Pacific Ocean (Larson & Hilde 1975; Cande *et al.* 1978; Channell *et al.* 1995). Moreover, M-anomaly GPTS have been difficult to calibrate owing to the scarcity of age constraints. The Larson & Hilde (1975) GPTS was calibrated using nannofossil zones from basal sediments recovered from Deep Sea Drilling Project (DSDP) cores, whereas the timescale by Channell *et al.* (1995) (hereafter CENT95) was calibrated indirectly with a radiometric age from MIT Guyot in the western Pacific and biostratigraphy and magnetostratigraphy in terrestrial strata.

The reliability of the M-anomaly GPTS can be improved by analysing a larger set of magnetic records from a wider region. In this study, we report a Pacific-wide M-anomaly model based on large numbers of carefully selected magnetic profiles from the three lineation sets on the Pacific Plate. We constructed our GPTS only from Pacific anomalies because the record is longer and more continuous in this region and because seafloor spreading rates in the Pacific were high and the sediment blanket is thin, translating to better spatial and temporal resolution. We restrict our analysis to anomalies from M0 to M29 because pre-M29 anomalies have been investigated only in the Japanese lineation set and the correlations are uncertain due to low amplitude, short wavelength anomalies that have not been widely confirmed (e.g. Sager *et al.* 1998; Tominaga *et al.* 2008).

1.1 Background

1.1.1 Distribution of M-anomalies

M-anomalies are identified in the oldest part of all three of the major ocean basins (e.g. Klitgord & Schouten 1986; Vogt *et al.* 1971a,b; Hayes & Rabinowitz 1975; Cooper *et al.* 1976; Verhoef & Scholten 1983; Roest *et al.* 1992; Sager *et al.* 1992; Ramana *et al.* 1994; Rybakov *et al.* 2000; Roeser *et al.* 2002; Ramana *et al.* 2001; Gurevich *et al.* 2006) (Fig. 1A). Most of these M-anomaly lineation groups do not show clear correlatability and repeatability in anomaly character due mainly to slow spreading rates (10–40 km Myr^{-1} half rate), thick sediments, and tectonic complications associated with fracture zones and continental breakup. The clearest extra-Pacific M-anomaly sequences occur to the northwest of Australia (Fullerton *et al.* 1989; Sager *et al.* 1992; Robb *et al.* 2005) where part of the sequence is found (M26–M16 and M10–M0), and in the north Atlantic (Vogt *et al.* 1971a,b) where the entire sequence is preserved.

The M-anomalies in northwest Australia and the north Atlantic have been extensively studied, but the clarity of anomaly character and continuity is less than those of the Pacific. Although the northwest Australia sequence shows similar anomaly characteristics to that of the Pacific anomalies, we cannot extract a complete, continuous sequence because these anomalies were recorded on two different ridges at different time periods with a time gap in between. In addition, the area contains numerous fracture zones, ridge jumps and major tectonic features including the Joey and Roo Rises and Exmouth Plateau (Fullerton *et al.* 1989; Robb *et al.* 2005).

Atlantic M-anomalies are observed in both the north and south Atlantic, but nearly complete M-anomaly sequences (M0–M25) occur only within the central north Atlantic crust. Although the north Atlantic anomaly sequences appear continuous, the resolution is less than that of the Pacific because seafloor spreading was slow at times and sediment thickness is large near continental margins (Vogt *et al.* 1971a,b), so that we can only identify larger anomalies. This is especially a problem for the older M-anomalies (>M21), which have low amplitudes that decrease backward in time (Cande *et al.* 1978). Furthermore, even though Sundvik & Larson (1988) and Schouten & Klitgord (1982) mapped M5–M16 off North America from dense aeromagnetic data, these anomalies are attenuated in amplitude and we cannot clearly identify them from existing sea-surface magnetic profiles. We believe that this 'smooth' zone resulted from the effect of slow spreading on the structure of the crustal magnetic source layer.

The three Pacific M-anomaly lineation sets are the Hawaii, Japanese and Phoenix (Fig. 2). They are isochrons of the expanding Mesozoic Pacific Plate formed at the Pacific-Izanagi, Pacific-Farallon and Pacific-Phoenix ridges, respectively (Nakanishi *et al.* 1989, 1992). The Hawaiian lineations have been used as the foundation of previous M-anomaly GPTS because they were the first identified complete lineation group and there are several subparallel, continuous magnetic survey lines that traverse the entire group (Larson & Hilde 1975; Nakanishi *et al.* 1989). The younger portion of the Hawaiian M-anomaly set is located near the west end of the Hawaiian seamounts (Hawaii 1 in Figs 2 and 3), and the older portion lies to the south of Shatsky Rise (Hawaii 2 in Figs 2 and 3). The Japanese lineation set is subducting at the northwest edge of the Pacific Plate in the Japan and Kuril Trenches, and into the Marianas Trench in the western Pacific (Fig. 2). The younger portion of the Japanese M-anomaly set is observed north of the Shatsky Rise (Japanese E and Japanese C in Figs 2 and 3) (Nakanishi *et al.* 1999), whereas the older portion of the Japanese M-anomalies is located in the east Mariana basin (Japanese W and S in Figs 2 and 3) (Handschumacher *et al.* 1988; Nakanishi *et al.* 1989). The younger portion of the Phoenix lineation set lies among many seamounts and fracture zones northeast of Ontong Java Plateau (Phoenix C in Figs 2 and 3) and the older portion is located in the Nauru Basin (Phoenix N in Figs 2 and 3). Although this area contains numerous tectonic complications, Nakanishi *et al.* (1992) identified almost the entire M-anomaly sequence in this group except for M0 and pre-M29 anomalies.

1.1.2 Development of the M-anomaly GPTS

The development of the M-anomaly GPTS occurred mainly with three studies, all of which used a small number of magnetic profiles covering a limited area. The Hawaiian M-anomaly model of Larson & Hilde (1975) was the foundation for most subsequent M-anomaly GPTS models. Their GPTS is a composite of seven segments of magnetic anomaly profiles from the Hawaiian lineations ("Hawaii 1" in Fig. 3). In this GPTS, ages of polarity boundaries were determined using a constant spreading rate and biostratigraphic ages for basal sediments overlying the igneous crust from DSDP holes in the Pacific and Atlantic.

Cande *et al.* (1978) added anomalies M26–M29 to the GPTS of Larson & Hilde (1975). Although they compared segments of 13 magnetic profiles from all three Pacific lineation sets, they used only one profile from the Japanese lineation set to construct the M26–M29 GPTS. Polarity boundary ages were extrapolated from Larson & Hilde (1975), assuming a constant spreading rate.

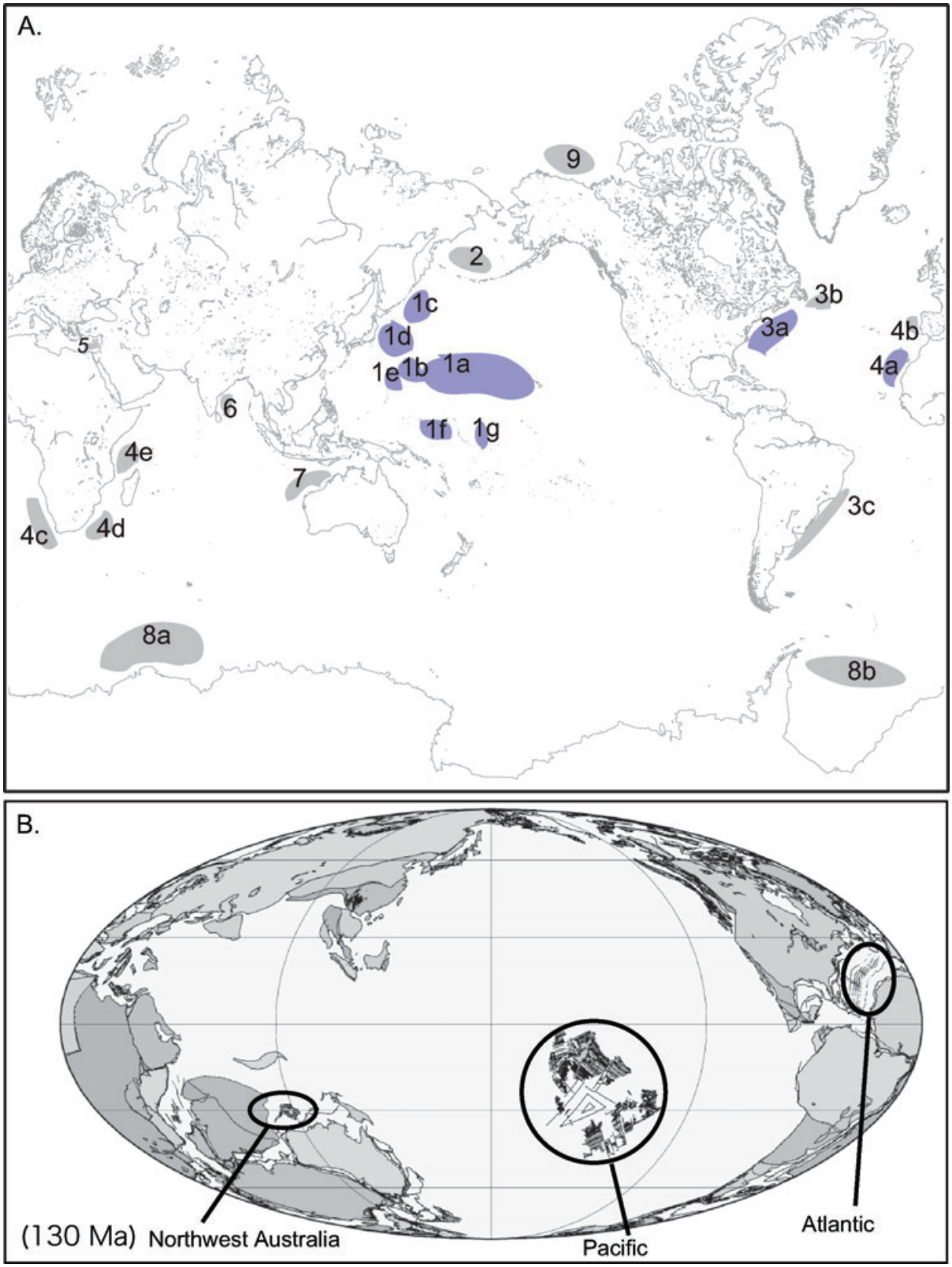

Figure 1. (A) Comprehensive map of M-anomalies reported from the ocean basins. Representative publications related to the regions are as follows: 1a–g, Pacific lineation set (detailed in Fig. 2); 2, Cooper *et al.* (1976); 3a–b = Vogt & Johnson (1971) and Vogt *et al.* (1971a,b); 3c, Rabinowitz & LaBreque (1979); 4a, Hayes & Rabinowitz (1975) and Roest *et al.* (1992); 4b, Whitmarsh *et al.* (2000); 4c, Milner *et al.* (1995) and Gladczenko *et al.* (1997); 4d, Plessis & Simpson (1974); 4e, Rabinowitz *et al.* (1983); 5, Rybakov *et al.* (2000); 6, Ramana *et al.* (1994) and Gaina *et al.* (2007); 7, Larson (1975), Larson (1977) and Robb *et al.* (2005); 8a, Ramana *et al.* (2001); 8b, Lawver *et al.* (1985); 9, Gurevich *et al.* (2006). (B) The locations of three major M-anomaly groups (Pacific, Northwest Australia and Atlantic) superimposed on the 130 Ma Earth (modified from The PLATES Project by University of Texas Institute for Geophysics. http://www.ig.utexas.edu/research/projects/plates/).

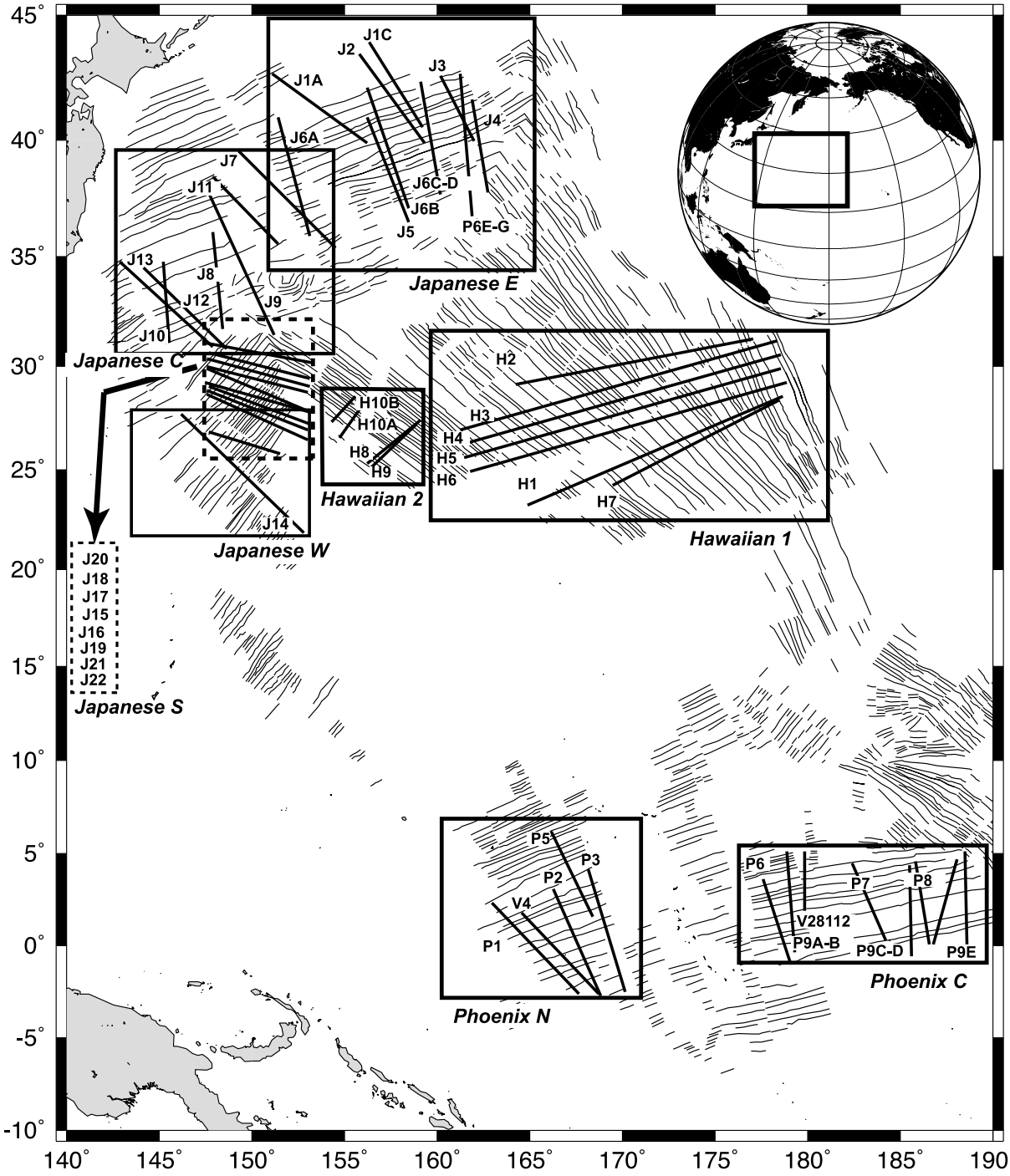

Figure 2. Locations of the Pacific M-anomaly lineation magnetic profiles. Each box shows the location of a group of profiles and the name of the lineation set is indicated. Track lines in each box correspond to those in Table 1 and Figs 3–9. Magnetic lineations (grey lines) are from Nakanishi *et al.* (1992).

CENT95 (Channell *et al.* 1995) was the first major revision of the M-anomaly GPTS. A total of 11 magnetic anomaly profiles from the three Pacific lineation sets were used to build polarity block models from M0 to M29 for each lineation set. Although the authors examined three calibration ages for the polarity sequence and modelled all three lineation sets, CENT95 is based on one profile from the Hawaiian lineations. Age calibration for CENT95 is based on dates of 121.0 and 154.0 Ma for M0 and M25, respectively, with linearly interpolated polarity chron ages in between. The Hawaiian lineation sequence was deemed the 'best' representation of the M-anomaly GPTS because the interpolation of these anomalies most closely matched a third radiometric age, 137.0 Ma, for M15–M16, a correlation from land stratigraphy.

Another widely cited GPTS is the Geological Time Scale book series (Harland *et al.* 1982, 1989; Gradstein *et al.* 2004). The most recent Geological Time Scale (Gradstein *et al.* 2004; hereafter TS2004) is a composite of three separate reversal models: the surface magnetic anomaly-based sequence from Hawaiian lineation set for M0–M24 (Larson & Hilde 1975), the aeromagnetic anomaly-based sequence from the Japanese lineation set for

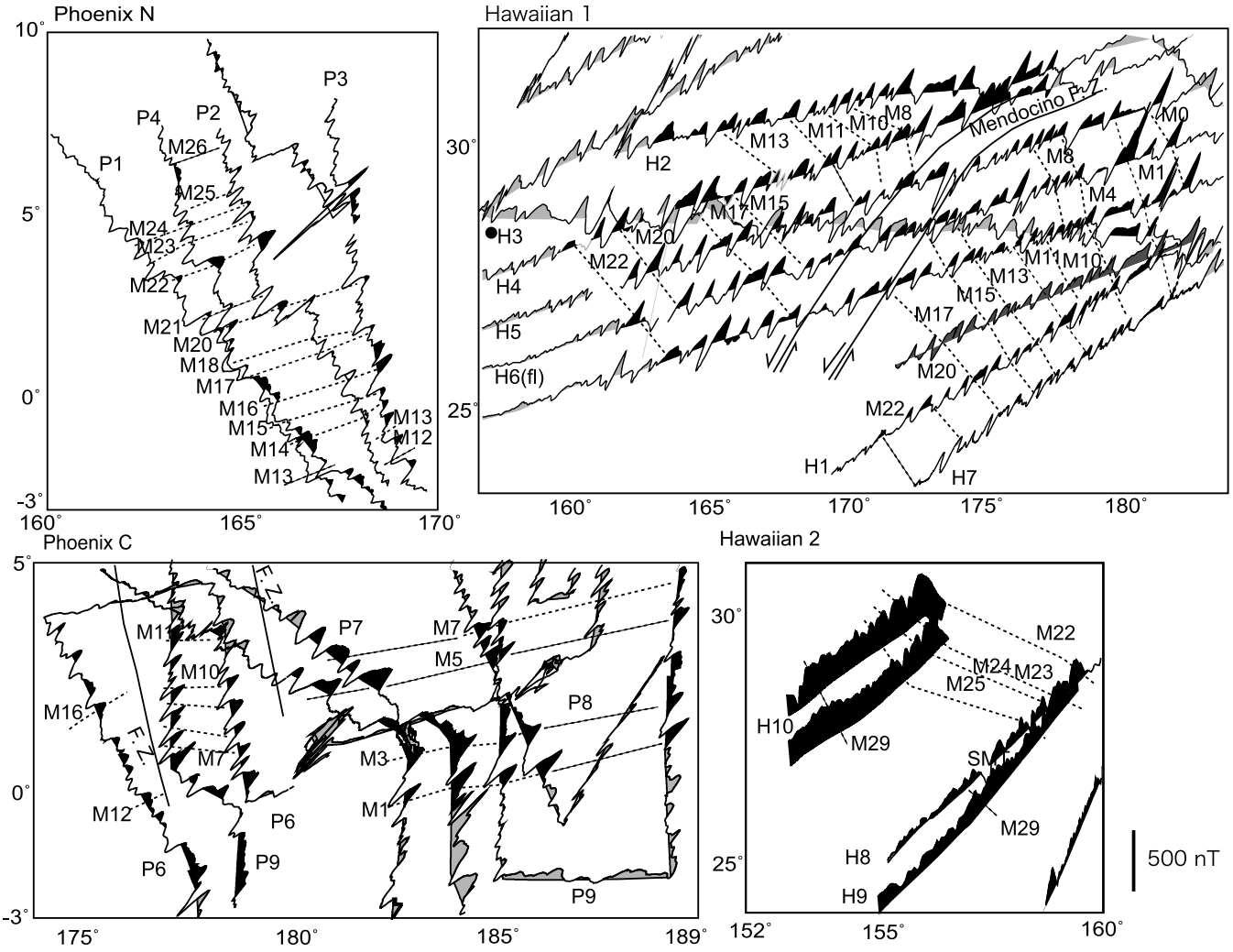

Figure 3. Correlation of anomalies on selected magnetic profiles. Anomaly profiles with positive anomalies shaded black were used for anomaly correlations in this study, whereas grey-shaded anomalies were not. Dotted lines indicate correlated anomaly peaks and troughs (e.g. Nakanishi *et al.* 1992). Part I. The regions Hawaiian 1, 2, Phoenix N, and Phoenix C (see Fig. 1). The profile IDs correspond to 'Index' in Table 1. The profiles H1, H3, H4, H5 and H6 in Hawaiian 1 are used in the Larson & Hilde (1975) and Channell *et al.* (1995) GPTS models. The profiles P1, P2 and P4 in Phoenix N, P6, P8 and P9 in Phoenix C, and H8, H9 and H10 in Hawaiian 2 are used for the anomaly correlations in Nakanishi *et al.* (1989, 1992). Part II. The regions Japanese C, E, W and S in Fig. 1. The profiles J7, J9, J10, J11, J12 and J13 in Japanese C, J1, J2, J3 and J6 in Japanese E, J14 in Japanese W, and J16, J17 and J18 in Japanese S are used for the anomaly correlations in Nakanishi *et al.* (1989, 1992). # symbol indicates newly identified occurrences of M0 in the Japanese lineations. F.Z., Fracture Zone; O.P., Ogasawara Plateau.

M25–M27n (Handshumacher *et al.* 1988), and a deep-tow magnetic anomaly-based sequence from Japanese lineation set for M27r–M29 (Sager *et al.* 1998). TS2004 uses a revised age for M0 (125.0 Ma) based on a suggested new global strato-type for M0 within terrestrial magnetostratigraphy and biostratigraphy (Channell *et al.* 2000).

The key radiometric dates used in these GPTS models have been changed. CENT95 used 121.0 Ma for M0 and 154.0 Ma for M26 with linearly interpolated ages for the rest of the polarity boundaries. The former date was inferred from terrestrial stratigraphy, which was later reinterpreted and shifted ∼4 Ma by Channell *et al.* (2000). The latter date was inferred from U-Pb and $^{40}Ar/^{39}Ar$ ages in Oxfordian-Kimmeridgian strata (Channell *et al.* 1995). The dates used in CENT95 were revised in TS2004. TS2004 used 125 Ma for M0 and 155.7 Ma for M26. In addition, TS2004 contains stratigraphic and radiometric ages for stage boundaries, tied to the reversal sequence by magnetic stratigraphy with interpolation in between those boundaries assuming a constant spreading in the Hawaiian lineations (Gradstein *et al.* 2005).

2 DATA AND METHODS

2.1 Selection of magnetic profiles

We distilled a total of 87 sea-surface magnetic profile segments from the Hawaiian, Japanese and Phoenix lineation sets in the Pacific using data from the National Geophysical Data Center (Fig. 3, Table 1), most of which were archived as anomaly values corrected to the International Geomagnetic Reference Field for various years. All the collected profiles have along-track bathymetry data and trend nearly perpendicular to previously determined magnetic lineation strikes. Those parts of the profiles that cross known fracture zones, ridge jumps that were suggested from previous anomaly

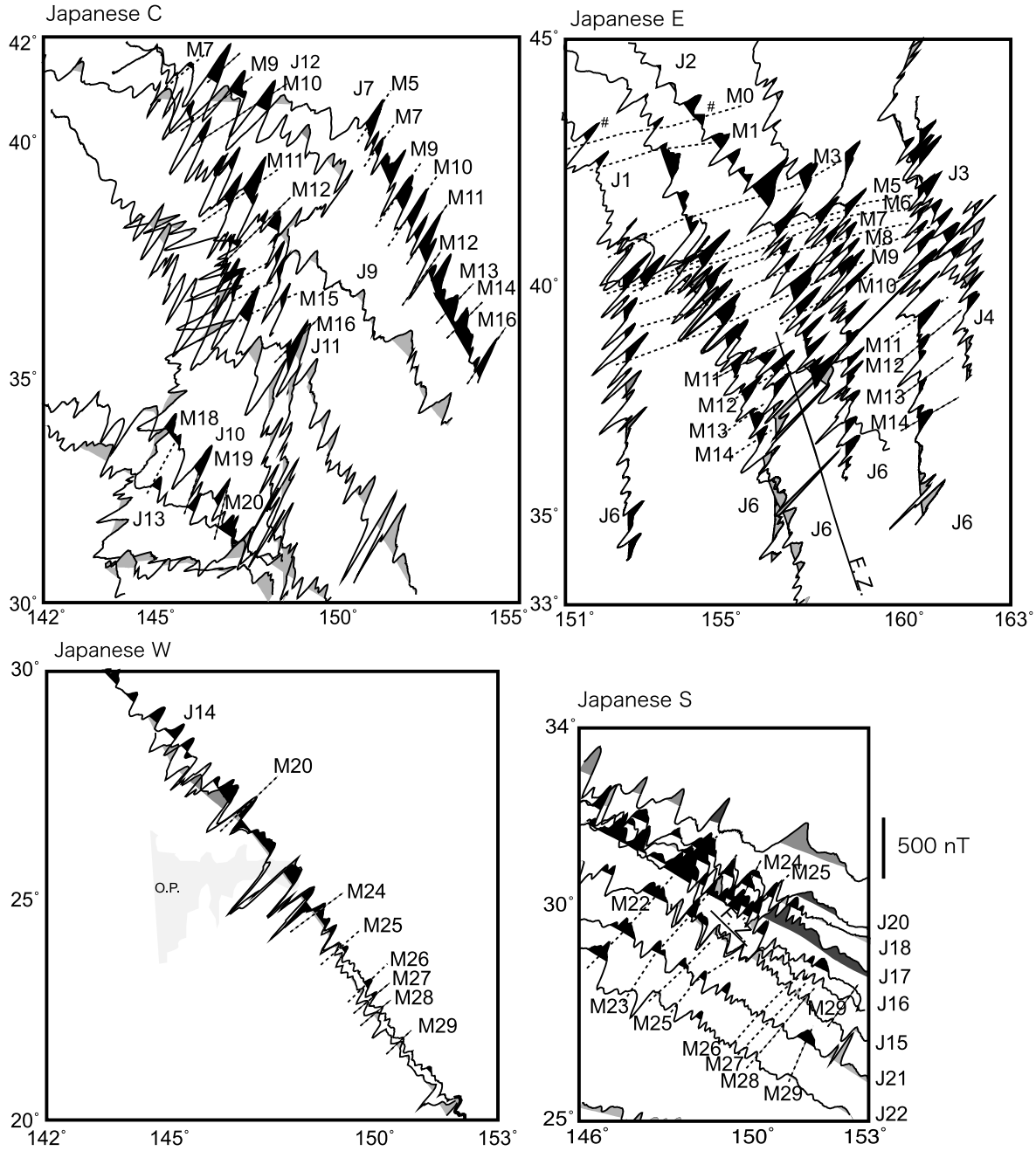

Figure 3. (*Continued*.)

correlations or seamounts and other bathymetric features, were ignored because these disturb the magnetic anomaly patterns. These criteria give profiles that show anomaly character most clearly, aiding in correlation, as well as providing the most repeatable set of anomalies.

2.2 Anomaly correlations

The collected profiles were grouped into five paleopole stages, M0–M4, M5–M10, M10N–M15, M15–M20 and M21–M29, for subsequent calculations (Figs 4–9). This grouping was necessary because (1) the anomaly sequence spans >1000 km and few magnetic profiles cross it entirely and (2) plate movement during the ∼30 Myr history of the M-anomalies changes the paleomagnetic parameters that determine anomaly skewness. These groups match the paleopole age groups in the paleomagnetic polar wander path of Larson & Sager (1992), allowing us to subdivide the sequence into approximately equal sections and to use those paleomagnetic poles to estimate paleomagnetic parameters. According to TS2004, the groups span ∼7 Myr (M0–M4), ∼4 Myr (M5–M10), ∼5 Myr (M10N–M15), ∼6 Myr (M15–M20) and ∼8 Myr (M21–M29).

Although our grouping of the anomalies in paleopole stages is similar to the method used in Cande & Kent (1992a), the purpose of this grouping is slightly different. Cande & Kent (1992a) grouped magnetic anomalies to calculate spreading rates and polarity durations using Euler poles. Their method was uniquely applicable to studies in the south Atlantic because the oceanic lithosphere evolved

Table 1. Magnetic profiles and magnetization parameters.

NGDC#	Cruise ID	Anomaly	Index	Site lat	Site lon	Pole lat	Pole lon	PI	PD	Slin
Hawaii 1										
1030095	V2404	M0	H1A	27.5	179.0	49.8	327.1	−15.1	20.1	150
		M5	H1B	27.0	178.0	48.3	322.2	−15.9	23.1	150
		M11	H1C	26.0	176.0	53.0	334.0	−17.0	13.2	150
		M16	H1D	25.0	173.0	60.4	321.5	−1.6	14.9	150
3040053	POL7004	M0	H2A	32.0	176.0	49.8	327.1	−8.5	18.2	150
		M5	H2B	31.5	173.0	48.3	322.2	−11.0	20.0	150
		M11	H2C	31.0	169.0	53.0	334.0	−9.9	8.9	150
		M16	H2D	30.5	165.0	60.4	321.5	5.8	11.3	150
3040057	POL7201	M1	H3A	32.0	176.0	49.8	327.1	−8.5	18.2	150
		M5	H3B	31.0	173.0	48.3	322.2	−11.9	20.0	150
		M11	H3C	30.5	169.0	53.0	334.0	−10.9	9.0	150
		M16	H3D	28.5	164.5	60.4	321.5	1.7	11.1	150
		M0	H4A	31.5	179.0	49.8	327.1	−7.8	19.9	150
		M5	H4B	30.5	176.0	48.3	322.2	−11.1	21.8	150
		M16	H4C	28.5	169.0	60.4	321.5	3.4	13.2	150
		M0	H5A	30.5	179.5	49.8	327.1	−9.3	20.3	150
		M5	H5B	29.5	176.0	48.3	322.2	−12.9	21.9	150
		M16	H5C	28.0	169.0	60.4	321.5	2.4	13.2	150
		M0	H6A	29.0	179.5	49.8	327.1	−12.1	20.4	150
		M5	H6B	28.0	176.0	48.3	322.2	−15.5	21.9	150
		M11	H6C	27.5	173.0	53.0	334.0	−15.3	11.4	150
		M16	H6D	26.5	169.0	60.4	321.5	−0.5	13.2	150
15040233	TUNE09WT	M0	H7A	26.5	179.5	49.8	327.1	−16.5	20.5	150
		M5	H7B	26.0	178.0	48.3	322.2	−17.7	23.2	150
		M11	H7C	25.0	176.0	53.0	334.0	−18.8	13.2	150
		M16	H7D	24.5	176.0	53.0	334.0	−19.7	13.2	158
Hawaii 2										
1030193	V3212	M22	H8	27.0	157.5	61	357.4	−1.0	−9.5	150
1030243	V3612	M22	H9	25.5	157.5	61	357.4	−3.9	−9.5	150
8010069	77031705	M22	H10A	28.5	155.0	61	357.4	2.7	−10.6	150
		M22	H10B	29.0	155.0	61	357.4	3.6	−10.6	150
Japanese E										
1010094	C1405	M0	J1A	42.0	152.0	48.3	322.2	1.4	6.5	70
		M0	J1B	42.0	155.0	48.3	322.2	2.0	8.5	70
		M0	J1C	41.0	157.5	48.3	322.2	0.6	10.1	70
1030055	V2006	M0	J2A	41.0	156.0	49.8	327.1	2.3	5.7	70
		M5	J2B	38.5	156.0	49.8	327.1	−2.7	5.7	70
1030073	V2110	M0	J3A	43.0	160.0	48.3	322.2	5.2	11.7	70
		M5	J3B	40.0	160.0	49.8	327.1	1.0	8.3	70
3040053	POL7004	M10	J4	40.0	162.0	53.0	334.0	6.5	13.0	70
15050030	DSDP32GC	M5	J5A	39.5	155.0	48.3	322.2	−2.9	8.5	70
		M11	J5B	36.0	156.5	53.0	334.0	−1.9	1.5	70
9030026	SI932005	M5	J6A	38.5	152.0	48.3	322.2	−5.5	6.5	70
		M5	J6B	39.0	155.0	48.3	322.2	−3.9	8.5	70
		M5	J6C	40.5	158.5	48.3	322.2	−0.1	10.7	70
		M11	J6D	37.5	158.5	53.0	334.0	1.2	2.7	70
		M2	J6E	42.0	160.5	49.8	327.1	5.1	8.6	70
		M5	J6F	40.5	160.5	48.3	322.2	0.5	12.0	70
		M11	J6G	37.5	160.5	53.0	334.0	1.3	3.9	70
Japanese C										
1010074	C1219	M5	J7A	39.5	151.5	48.3	322.2	−3.6	6.2	70
		M11	J7B	36.5	153.0	53.0	334.0	−0.9	−0.6	70
1010167	C2004	M10	J8	31.0	145.0	53.0	334.0	3.6	10.6	70
1030193	V3212	M10	J9A	39.0	147.0	53.0	334.0	4.3	−4.2	70
		M16	J9B	33.0	150.0	60.4	321.5	3.6	10.6	70
1030195	V3214	M17	J10	38.0	153.0	60.4	321.5	17.3	5.7	70
1030211	V3311	M10	J11A	37.5	149.5	53.0	334.0	1.2	−2.7	70
		M10	J11B	34.5	149.0	53.0	334.0	−4.7	−3.0	70

Table 1. (*Continued.*)

NGDC#	Cruise ID	Anomaly	Index	Site lat	Site lon	Pole lat	Pole lon	PI	PD	Slin
15010075	ZTES04AR	M13	J12A	37.0	149.0	48.5	322.2	−8.5	4.5	70
		M16	J12B	37.5	149.5	60.4	321.5	15.9	−3.9	70
		M6	J12C	40.0	148.0	48.5	322.2	−2.7	3.8	70
15060015	JPYN04BD	M18	J13	32.0	145.0	60.4	321.5	4.8	1.7	70
Japanese W										
15050089	DSDP89GC	M24	J14	23.5	150.0	61.0	357.4	−5.2	−12.9	70
Japanese S										
15050018	DSDP20GC	M22	J15	29.5	150.0	61.0	357.4	6.4	−12.9	70
15060015	JPYN04BD	M21	J16	30.0	150.0	61.0	357.4	7.4	−12.9	70
J2010012	GH7901	M21	J17	30.0	150.0	61.0	357.4	7.4	−12.9	70
J2010018	GH805-A	M21	J18	30.5	150.0	61.0	357.4	8.3	−12.9	70
J2010019	GH805B	M21	J19	29.5	150.0	61.0	357.4	6.4	−12.9	70
J2010022	GH771-C	M21	J20	31.0	150.0	61.0	357.4	9.3	−12.9	70
J2010023	GH824-A	M21	J21	27.5	150.0	61.0	357.4	2.5	−12.9	70
J2010024	GH824-B	M21	J22	26.5	150.0	61.0	357.4	0.5	−12.9	70
Phoenix N										
1010060	C1205	M11	P1A	−1.0	164.0	53.0	334.0	−56.7	7.4	260
		M16	P1B	1.0	164.0	53.0	334.0	−54.8	7.4	260
1030195	V3214	M14	P2A	0.0	167.5	60.4	321.5	−44.7	13.9	260
		M21	P2B	5.0	165.5	53.0	334.0	−50.4	8.1	260
15080020	NOVA1AHO	M10	P3A	0.0	169.0	60.4	321.5	−44.3	14.7	260
		M15	P3B	1.0	169.0	53.0	334.0	−54.8	7.4	260
1030215	V3401	M10	P4A	−0.5	166.0	60.4	321.5	−45.8	13.3	260
		M16	P4B	1.0	164.0	53.0	334.0	−54.8	7.4	260
		M22	P4C	4.5	164.0	61.0	357.4	−41.2	−7.0	260
		M22	P5	7.0	166.0	61.0	357.4	−38.1	−5.9	260
Phoenix C										
1030139	V2811	M5	P6A	1.0	176.0	48.3	322.2	−52.0	26.1	260
		M10	P6B	1.0	176.0	48.3	322.2	−52.0	26.1	260
		M12	P6C	2.0	178.5	53.0	334.0	−50.5	16.9	260
		M15	P6D	2.5	174.0	53.0	334.0	−51.3	14.0	260
15040185	RNDB13WT	M1	P7A	−1.0	182.0	49.8	327.1	−52.2	26.1	260
15040031	7TOW3BWT	M1	P8A	1.5	185.5	49.8	327.1	−48.0	27.3	260
		M5	P8B	4.0	184.5	48.3	322.2	−44.3	29.9	260
		M1	P8C	1.5	187.5	49.8	327.1	−46.9	28.3	260
1010079	C1304	M1	P9A	3.0	189.0	49.8	327.1	−44.4	28.7	260
		M5	P9B	1.0	189.0	48.3	322.2	−44.6	32.7	260
		M1	P9C	3.0	184.0	49.8	327.1	−45.2	30.3	260
		M5	P9D	2.5	184.8	48.3	322.2	−45.7	30.4	260
		M5	P9E	2.0	177.5	49.8	327.1	−51.3	22.6	260

NGDC#, NGDC archive number; ID, survey ID in NGDC archive; anomaly, a chron number in which approximately an anomaly profile starts; index, profile ID indicated on Figure 4 and segment ID indicated in Figs 5–9; site lat, latitude of a middle point on a given magnetic profile segment; site lon, longitude of a middle point on a given magnetic profile segment; pole lat, paleo pole latitude; pole lon, paleo pole longitude; PI, paleo inclination of a given profile; PD, paleo declination of a given profile; slin, track line azimuth from north towards young direction of the lienation.

nearly symmetrically on conjugate sides of the Mid-Atlantic Ridge and without significant changes in latitude (Cande & Kent 1976; Cande & Kent 1992a). Determining spreading rates using Euler poles was not feasible in the Pacific because we could not model anomalies along a single flow line between fracture zones as did Cande & Kent (1992a). We used the age grouping to obtain paleoinclination and paleodeclination parameters for each paleopole stage that are used to deskew the magnetic profiles in subsequent polarity block modelling.

Each age group includes 16–21 anomaly profiles, with data from all three lineation sets. To provide consistent distances, all of the profiles were projected perpendicular to the local strike of the magnetic lineations. We made preliminary correlations of peaks and troughs of the anomalies among those in each age group, referring to correlations from previous studies (Larson & Hilde 1975; Nakanishi *et al.* 1989, 1992; Channell *et al.* 1995) (Fig. 3).

2.3 Polarity block modelling

After the correlation and identification of anomalies, we sought to derive an accurate and robust M-anomaly polarity block model assuming that the correlated anomalies result from blocks of alternating polarity in the upper crust. To prepare for subsequent calculations, we resampled both along-track bathymetry and magnetic anomaly profiles into equally spaced data (0.1 km interval), which are needed for the Fourier transform in the inverse modelling.

A polarity block model was built for each profile using both inverse and forward modelling. Inverse modelling (Parker & Huestis

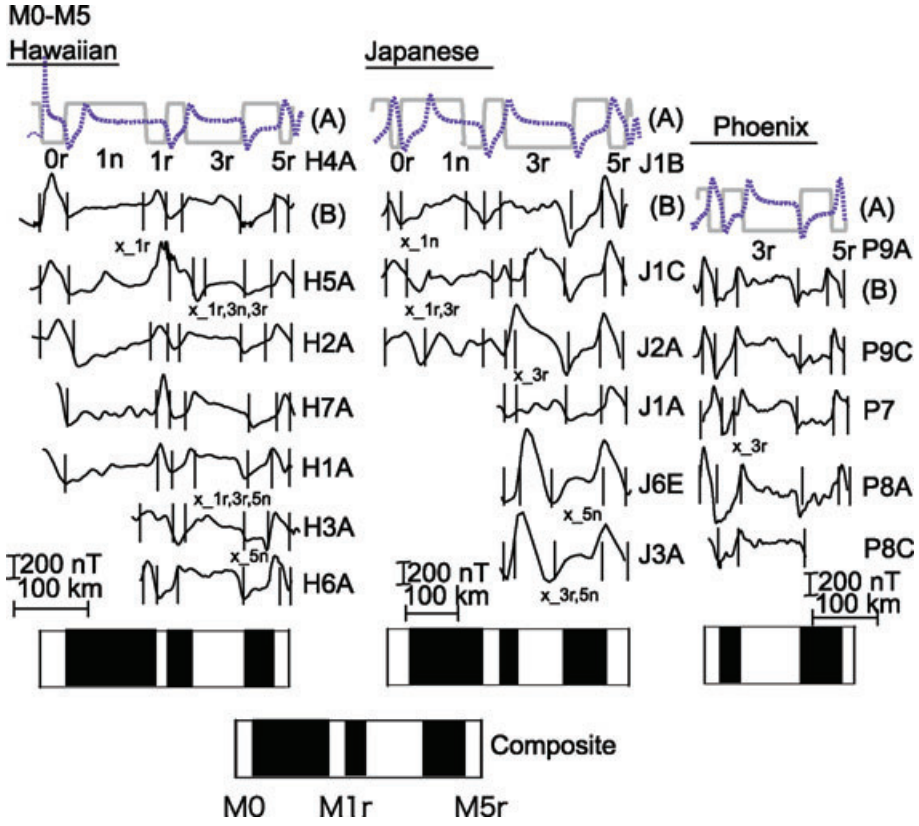

Figure 4. M0–M5n magnetic anomaly profiles and correlations. The profiles are projected with a common azimuth perpendicular to lineation trend. Each anomaly segment is annotated by a cruise identification (Table 1 and Fig. 2). (H), Hawaiian lineation set; (J), Japanese lineation set and (P), Phoenix lineation set. Top pair of profiles in each column show an example profile and model. (A) The polarity model (grey) and calculated anomaly (dotted line), whereas (B) the observed anomaly and the boundary of the first positive in each major chron (vertical bars). Note that, for clarity, not all chron boundaries are shown. The black and white stripe bars below the profiles show the averaged polarity block model from each lineation set. The polarity block model located at the bottom of the figure represents the composite model from all three lineation sets (see text and Figs 10 and 12). The combination of numbers (1, 2, 3, . . .) and letters of r (reverse) and n (normal) displayed next to x_ indicates the rejected (x) polarity boundaries in the magnetic profiles shown above the x_ indicator. These rejected polarity boundaries are following our selection criteria (see details in Section 2.4)

1974) was used as an objective method to obtain a preliminary model of polarity zones. The inverse modelling outputs a magnetization distribution along the magnetic anomaly profile (Fig. 10, A1–A2, Parker & Huestis 1974). We used this magnetization distribution to make a preliminary estimate of boundaries of opposite polarity blocks. These, in turn, were used as input for a forward modelling (Fig. 10, A2–A3). For the forward model, the preliminary estimated polarity block boundary locations were manually shifted until the forward modelling resulted in a good match to the observed anomalies. The polarity block model in the forward modelling was Gaussian filtered ($\sigma = 10$ km in the Gaussian distribution equation) to give smooth, finite-width polarity transitions and a better match of calculated and observed anomalies (Fig. 10, A3). The reason that we did not use the inverse model to estimate final model polarity boundaries was that the boundary locations could be affected by anomaly base level (i.e. the annihilator function) and the frequency content of the anomalies. For the Pacific, this two-step method yields somewhat more reliable boundary locations as compared with simply using anomaly zero-crossings (*cf*. Cande & Kent 1992a). This is because the M-anomaly sequences can contain gradual changes in amplitude (e.g. Cande *et al.* 1978) that can offset the zero crossings.

For both inverse and forward modelling, the magnetic anomalies were bandpass filtered to retain wavelengths between of 3 and 140 km. The rationale is that longer and shorter wavelength variations do not represent seafloor spreading magnetic anomalies. An annihilator function of zero was used under the assumption of approximately equal normal and reversed polarity. To account for anomaly asymmetry (skewness) in inverse and forward modelling, model calculations used values for the remanent magnetization (paleoinclination and paleodeclination) inferred from the contemporaneous paleomagnetic pole (Table 1) from Larson & Sager (1992). We chose the Larson & Sager (1992) paleopoles calculated without anomalous skewness because anomalous skewness apparently becomes negligible at spreading rates above 50 km Myr^{-1} (Dyment *et al.* 1994), which are typical of the Pacific Plate spreading. To define the depth of the magnetic source layer, we used along-track bathymetry data to give ocean depth. Sediment thickness was assumed to be constant at 0.3 km because this value is a crude average for the western Pacific (e.g. Abrams *et al.* 1992), where sediments are usually thin and do not vary greatly in thickness (see http://www.ngdc.noaa.gov/mgg/sedthick/sedthick.html). Errors in depth-to-source resulting from this assumption will be at most a few hundred meters and will have a negligible effect on the final model.

We did not use the downward continuation step used by Cande & Kent (1992a) to accentuate short wavelength features in the anomaly profiles. This procedure could result in misidentification of

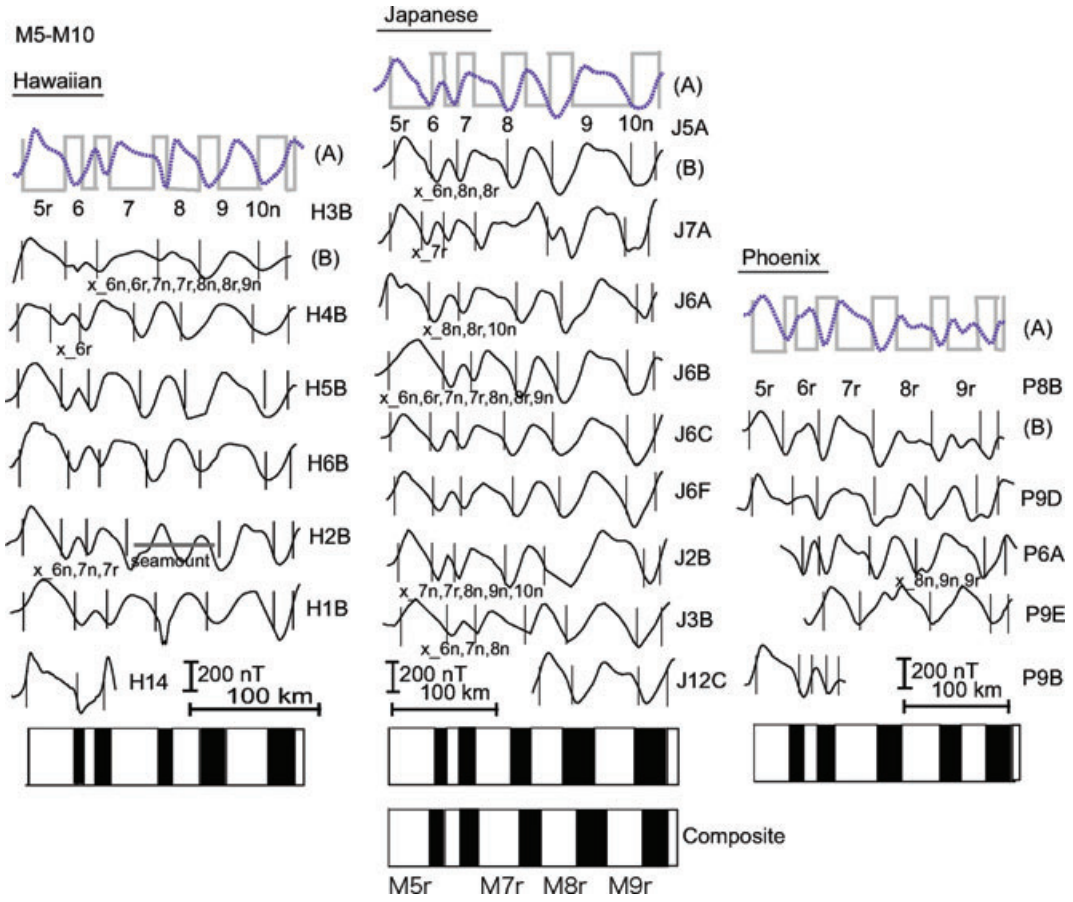

Figure 5. M5r–M10r magnetic anomaly profiles and correlations. Plot conventions as in Fig. 4.

subchrons, particularly in the low amplitude M-anomaly profiles, because high wavenumbers, including noise, are enhanced (Gubbins 2004). In the Pacific, the anomalies are recorded by fast spreading crust, which retains many small anomalies, and downward continuation was unnecessary.

2.4 Building average polarity block models for each age group

We determined the location of each polarity boundary in each age group by averaging normalized locations of the boundaries. The polarity block model from each magnetic profile segment was normalized to the distance between the group end anomalies (e.g. M0–M5n etc.). This normalization process is essential for comparing profiles at different spreading rates because we could not restrict anomalies to single flow line and spreading rates were different on each of the ridges and often varied along ridge strike (e.g. Nakanishi *et al.* 1989, 1992).

The normalized polarity boundary locations from each magnetic profile segment were averaged to build an average block model for each age group and for each lineation set. Each magnetic profile segment produced a series of polarity block boundaries each of which represents a magnetic reversal, $r_1, r_2, \ldots, r_n$, where n is the number of boundaries. Normalized to the group width, each reversal boundary becomes a percentage, p_i, yielding the sequence $p_1, p_2, \ldots, p_n$. With m observations of a particular boundary, its average position in the series is simply

$$\bar{p}_i = \frac{\sum_{i=1,m} p_i}{m}.$$

Thus, the end result of the age group averaging is a series of average block boundary positions, $\bar{p}_1, \bar{p}_2, \ldots, \bar{p}_n$, where$p$ is in scaled distance. When a profile segment did not span the entire length of a pole stage, the ends of the profile segment were tied to intermediate anomalies within one continuous profile in that spanned the entire age group.

In averaging the locations of polarity boundaries from each normalized magnetic profile segment in a age group, we refined the average of each polarity boundary location by excluding values outside the 95 per cent confidence limits and recalculating the average and its standard deviation (Table 2). This step was used to prevent bias in the polarity boundary average locations by outliers. This method of rejecting outlier data is superior to that of simply rejecting 'anomalous' profiles wholesale because it allows us to retain information from consistent anomalies in otherwise problematic profiles. The 95 per cent confidence limits for each boundary location were calculated using a t-distribution because the number of samples is often small ($m < 30$), and the distribution may not be Gaussian, so using the t-value is potentially a more accurate method. As shown in Fig. 11, the outlier rejection process significantly reduced the uncertainty of boundary locations in the Hawaiian and Japanese profiles. The uncertainty distribution was nearly unchanged for the Phoenix profiles, presumably because of greater variability in the polarity boundary locations of those

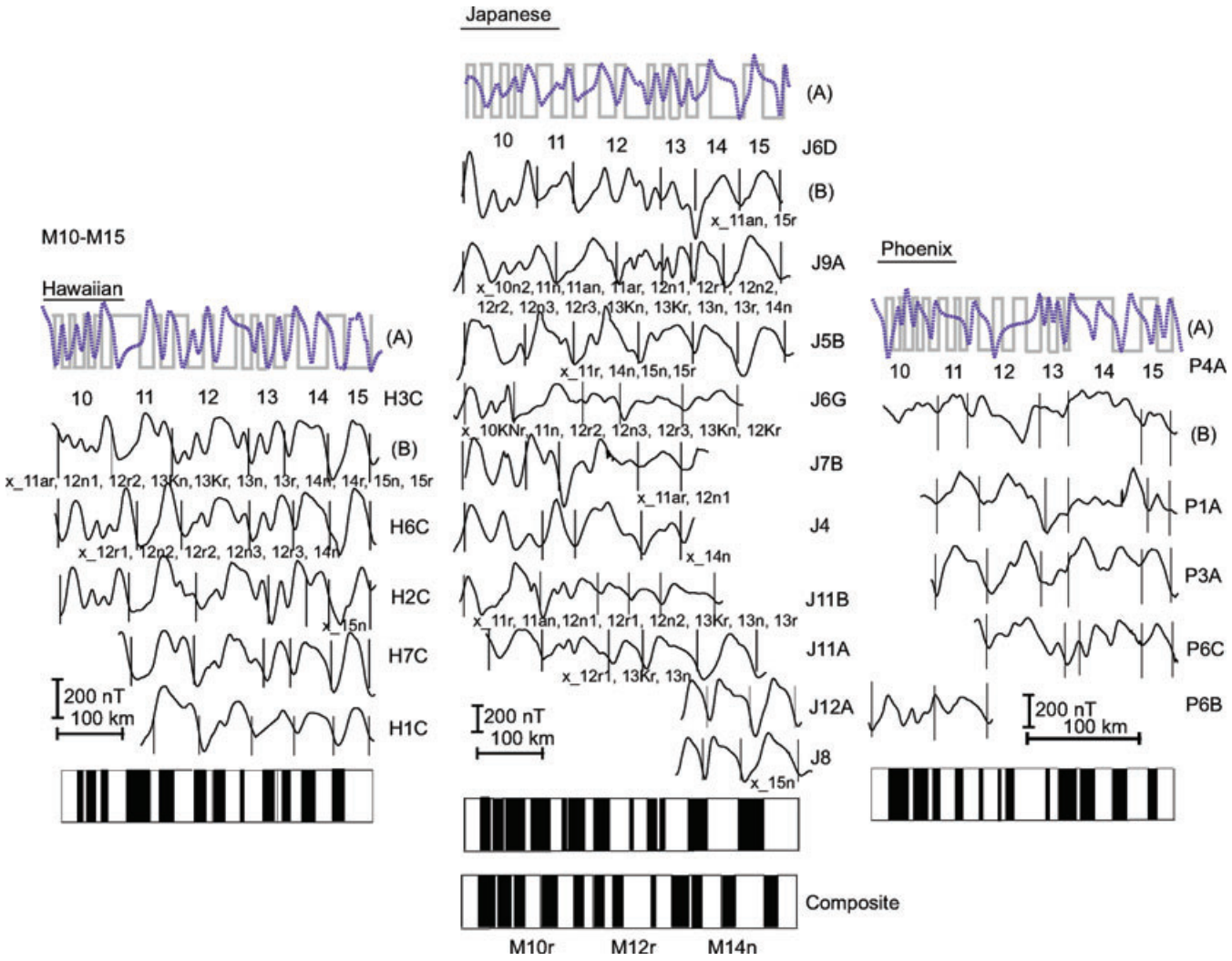

Figure 6. M10N–M15r magnetic anomaly profiles and correlations. Plot conventions as in Fig. 4. Subchrons within M10, M11, M12 and M13 are magnified vertically and indicated with arrows in the inset boxes in Fig. 9.

lineations, resulting from tectonic complications (e.g. Nakanishi *et al.* 1992).

2.5 Building complete polarity block sequences

We built a complete polarity block sequence model for each lineation set by concatenating the averaged polarity block models from the five age groups. This was done first for each lineation set, so we could compare each lineation set with the others, and then those models were averaged for a Pacific-wide model.

To combine the pole stage sequences into a total polarity block sequence model for each lineation set, we need to know what percentage of the total GPTS length is spanned by each of the five age groups. This information varies with each profile was lost by dividing the anomalies into different groups and normalizing. To accomplish this scaling, we determine the average position of each of the pole group end anomalies (i.e. M5, M10N, M15 and M20) relative to the entire anomaly sequence (M0–M29), based on an average of the positions of these anomalies in selected reference magnetic profiles. For the reference lines, we chose profiles that contain the most continuous and clear magnetic sequences. Profiles NOAA1-4 were used as reference profiles for the Hawaiian anomalies; profiles V2006, V2110, C1219, DSDP32, V3212, GH7901 and GH805 were used for the Japanese anomalies; and profiles V3401, V3214, C1205, NOVA1AHO and C1304 were used for the Phoenix anomalies (see also Fig. 3 and Table 1). For both the Japanese and Phoenix lineations, it was necessary to connect two to three reference profiles because there is no single profile that covers the entire M0–M29 sequence in these lineation sets. We thus combined these profiles into a composite reference line by scaling one profile to the other using overlapped sequences around M5 and M16 for the Japanese reference profile and around M7, M11 and M16 for Phoenix reference profile.

To combine the average polarity block models for each lineation set into a Pacific-wide composite, we averaged the block boundaries from each model based on their position in the total block sequence for each lineation set. In addition to the Pacific-wide model, we also built a composite model using only the Hawaiian and Japanese lineation sets because of concern that the higher variability in the Phoenix block model may adversely affect the composite model. As we describe in the discussion, however, this Phoenix-less model provided no significant improvement (Figs 12A and 13).

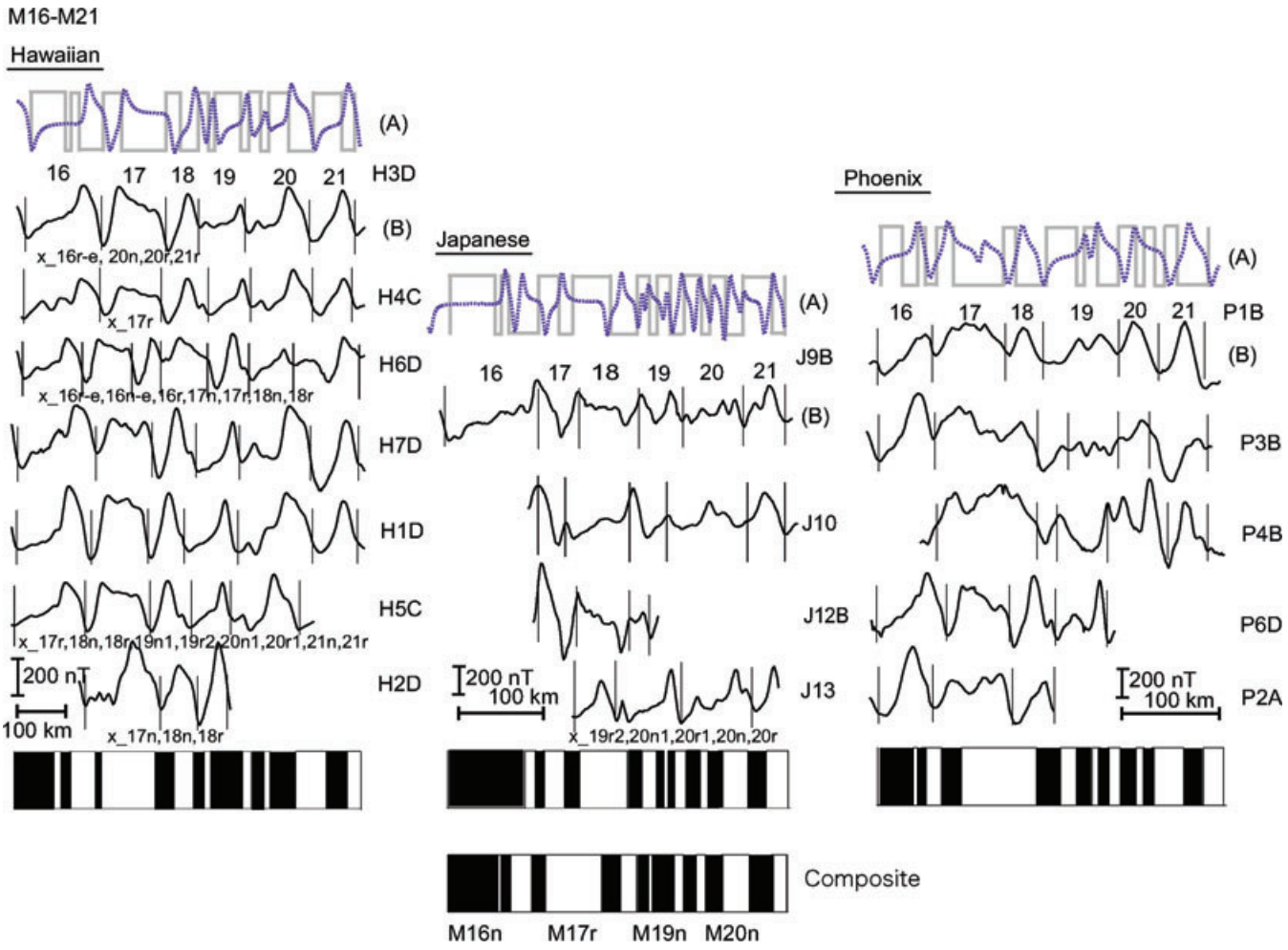

Figure 7. M16n–M20r magnetic anomaly profiles and correlations. Plot conventions as in Fig. 4. Subchrons in M16, M1 and M20 are magnified vertically and indicated with arrows in the inset boxes in Fig. 9.

2.6 Age calibration for timescale model

Few radiometric ages are available for the M-anomalies (e.g. Pálfy *et al.* 2000) and most are not directly connected to marine magnetic anomalies (e.g. Gradstein *et al.* 1995). Because we could not find any reliable direct dates for the middle of the polarity sequence, we used only two age calibration points, one at each end of the anomaly sequence. For the old end, we used 155.7 $\pm$ 3.4 Ma for the base of the M26r, a date from rocks cored on M26 in the Argo Abyssal Plain (Ludden 1992). At the young end of the sequence, we have adopted 125.0 Ma for the base of M0r, that is the age of the Aptian-Barremian stage boundary by Channell *et al.* (2000). Given the poor age constraints for the M-anomalies, a simple linear interpolation is appropriate.

3 RESULTS

3.1 Anomaly correlation

Overall, correlations of anomalies within each lineation set were readily made because the anomalies are mostly coherent in shape and amplitude for the entire M0–M29 period. Anomaly shapes compared among lineation sets have only minor differences, which show up mainly in M19, M20 and M25–M29 (Figs 7–9). This high repeatability among all three lineation sets implies that the modelled polarity chrons reflect Pacific-wide geomagnetic behaviour. In this section, we describe differences in chron and subchron correlations (Figs 4–8) with respect to previous studies. Most of the differences are in the interpretation of secondary anomalies.

We identified M0 in the Japanese lineation set (Figs 3 and 4) on two profiles near the Japan Trench. Although M0 was not recognized in the Japanese lineation set by Nakanishi *et al.* (1989), on these two profiles it compares well to the expected shape and spacing with M0 in the Hawaiian lineation set. The broad normal and reverse polarity sequence of M1r and M3n are also characteristic features easily recognized in many profiles in this region (Fig. 4).

In previous studies of the M-anomalies, there has been no consistent treatment of small anomalies and the polarity subchrons that they represent in the reversal model. To be included in our model, any small anomaly had to pass the following criterion: it was identified on >50 per cent of the total available profiles and recognized in all three lineation sets. This indicates that the anomaly is a global, repeatable feature (Fig. 9). Because of this criterion, we dropped one subchron anomaly from the previous M11 and M24 correlations (Channell *et al.* 1995) and we added one anomaly each to M13 and M16. Our correlations showed that one of the two previously identified correlated anomalies in M11 is

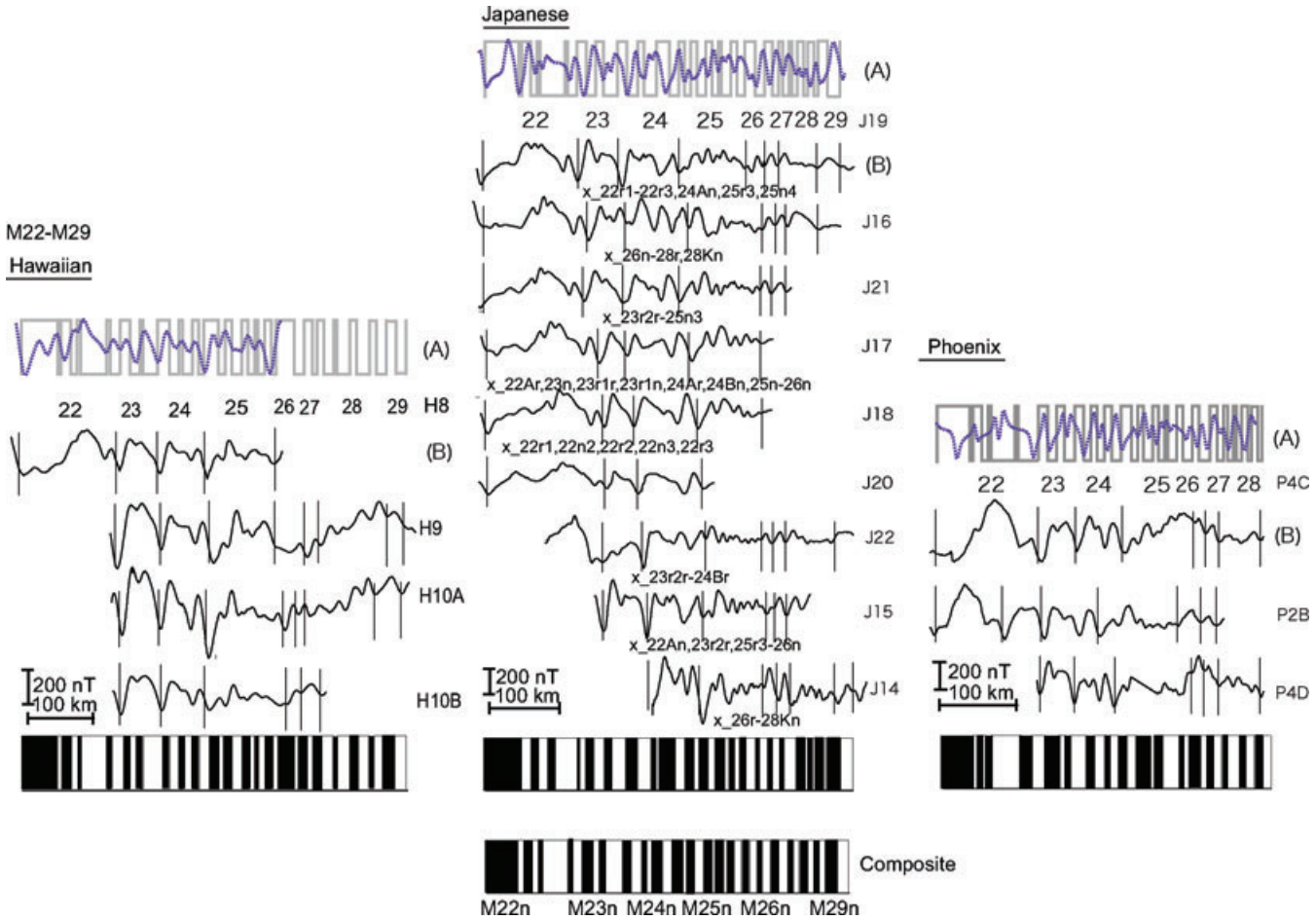

Figure 8. M21n–M29r magnetic anomaly profiles and correlations. Plot conventions as in Fig. 4. Subchrons within M22, M23, M24 and M25 are magnified vertically and indicated with arrows in the inset boxes in Fig. 9.

observed only on profiles POL7004 and DSDP32GC (H2C and J5B in Fig. 9), whereas the other is confirmed by the Pacific-wide correlation. This subchron was probably retained in previous studies because it occurs on profile POL7004, which is one of those used by Larson & Hilde (1975) to define the M-anomalies. A new subchron within M13n, not reported previously, is recognized in all three lineation sets and numbered M13n.1r (f in Figs 6 and 9). We also propose a new subchron in M16n, which divides that normal polarity block and results in the pair M16n.1r and M16n.2n (g in Fig. 9). This subchron has not been reported in previous studies but is observed in all three lineation sets. Although the anomaly amplitude is low for this subchron it is similar to previously identified small anomaly features in other chrons (e.g. M19.n1 and M20.n1, h and i in Fig. 9).

For the age group M21–M29, anomaly correlation is more difficult than in younger anomalies because anomaly amplitudes decrease with increasing age past M21. Although CENT95 contains four pairs of normal and reversed blocks within M24, our model retains only two pairs. The difference can be attributed to the fact that the extra subchrons in CENT95 are interpreted from short wavelength, small amplitude anomalies observed only on a few magnetic profiles in the Hawaiian lineation set. Anomalies prior to M24 become even more difficult to identify due to their low amplitudes. Nevertheless, we identified the previously suggested anomalies prior to M24 on 15 magnetic profiles (Fig. 8), so we consider that the model sequence represents correlatable anomaly features that are consistent with the chrons and subchrons suggested in previous studies (Nakanishi *et al.* 1989, 1992). Our model contains two more subchrons in M25, and one less in M28 compared to those in TS2004 (Gradstein *et al.* 2005). This difference occurs because TS2004 used different data sets: aeromagnetic data for M25–27 (Handshumacher *et al.* 1988) and deep-towed magnetic data (Sager *et al.* 1998) for pre-M28 anomalies.

3.2 Variability in location of polarity boundaries

Average block models for each age group from all three lineation sets and their composite models are shown in Figs 4–8. Overall, the distribution of polarity boundaries among the three lineation sets for each age group is nearly identical, suggesting that there is little variability in the polarity reversal records in crust on different ridges with different spreading rates. Model variability is least in the sequence M0–M10 where polarity boundaries in stacked profiles line up closely (Figs 4–5). The highest variability is observed in M11–M15 (Fig. 6). Although the repeatability of the anomaly sequence is convincing, there is a greater variability of anomaly widths and more instances where an anomaly on a given profile may not appear with its characteristic shape. Anomalies M16–M21 show somewhat greater regularity (Fig. 7), especially within the Hawaiian anomalies. Anomalies M21–M24 appear quite regular in all lineation sets (Figs 7 and 8). Despite the fact that the small

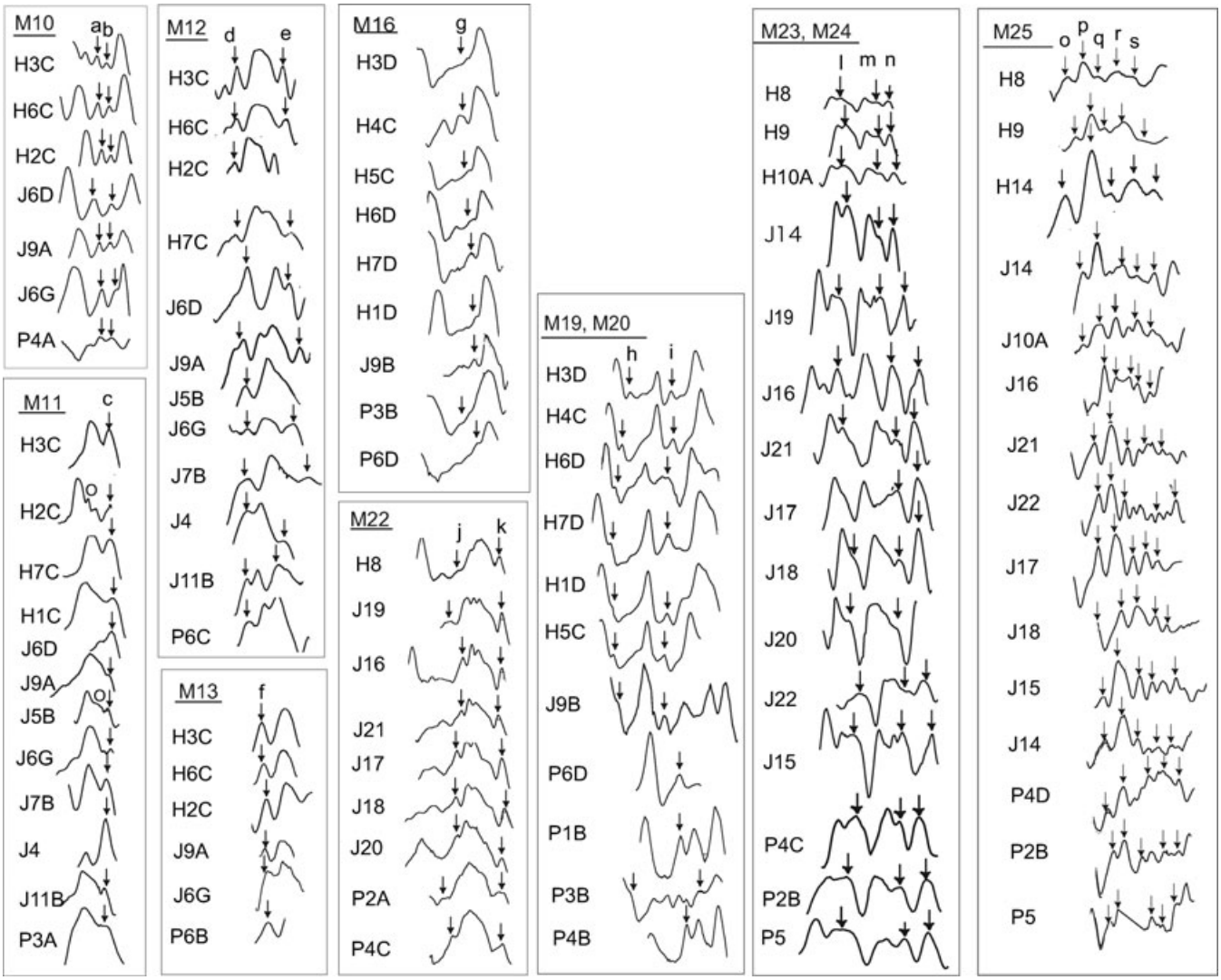

Figure 9. Subchrons identified within major chrons. The parental anomaly correlations are shown in Figs 3–7. The open circles indicate dropped subchrons. For reference, the arrows indicate subchron anomalies as follows: M10-a,-b are M10Nn.1 and M10Nn.2; M11-c is M11r; M12-d,-e are M12n and M12A; M13-f is M13n.1r; M16-g is M16n.1r; M19-h is M19n.1r; M20-i is M20n.1r; M22-j is M22n.2; M22-k is M22A; M23-l is M23r.2r; M24-m is M24r.2r; M24-n is M24Ar and M25-o–M25-s are five subchrons identified in M25 (Table 1).

amplitude M25 and older anomalies are more difficult to correlate, the modelled polarity boundaries show remarkably little variation (Fig. 8).

Variation in polarity block model spacing is apparent when composite models for each lineation set are compared (Fig. 12A). Little difference is seen from M0 to M15 between the Japanese and Hawaiian blocks. The average Hawaiian model is slightly expanded relative to the Japanese model, but both Hawaiian and Japanese blocks are expanded relative to the Phoenix blocks. From M15 to M21, the Japanese blocks partly catch up to the Hawaiian blocks whereas both Japanese and Hawaiian blocks maintain a lead over the Phoenix blocks. The differences disappear towards the end of the polarity model sequences, particularly in between M25 and M29, as the models are all constrained to the end point of 100 per cent. These model differences are highlighted by plotting the polarity block distances (in percentage) for two of the three lineation set models one against the other (Fig. 12B). The Japanese–Hawaii comparison produces the least deviation from a straight diagonal (a perfect match), with only a small difference for the period of M13–M15. In contrast, the Phoenix–Hawaii and Phoenix–Japanese comparisons plot above the diagonal (i.e. Hawaiian and Japanese sequences are more expanded) until about M8, after which the models produce little deviation from a straight diagonal.

3.3 Modelling uncertainty

Standard deviations of model polarity boundary locations were first determined in dimensionless percentage, but were translated into kilometers with the mapping of the model onto the reference anomaly profiles. Polarity boundary location uncertainties show a range of 7–17 km (Table 3). To calculate the corresponding uncertainty in polarity zone widths, for comparison with the results of Cande & Kent (1992a), we use values from two, neighbouring boundaries, defining the polarity zone widths: $w_i = p_{i+1} - p_i$ and $\sigma_i = \sqrt{\sigma_i^2 + \sigma_{i+1}^2}$ where s_i is the standard deviation of p_i. The polarity zone width standard deviations range 2–36 km (average 11 km) for the Hawaiian model, 1–36 km (14 km) for the Japanese model and 2–33 km (9 km) for the Phoenix model. These values are similar to those from the model of Cande and Kent (1992), suggesting that

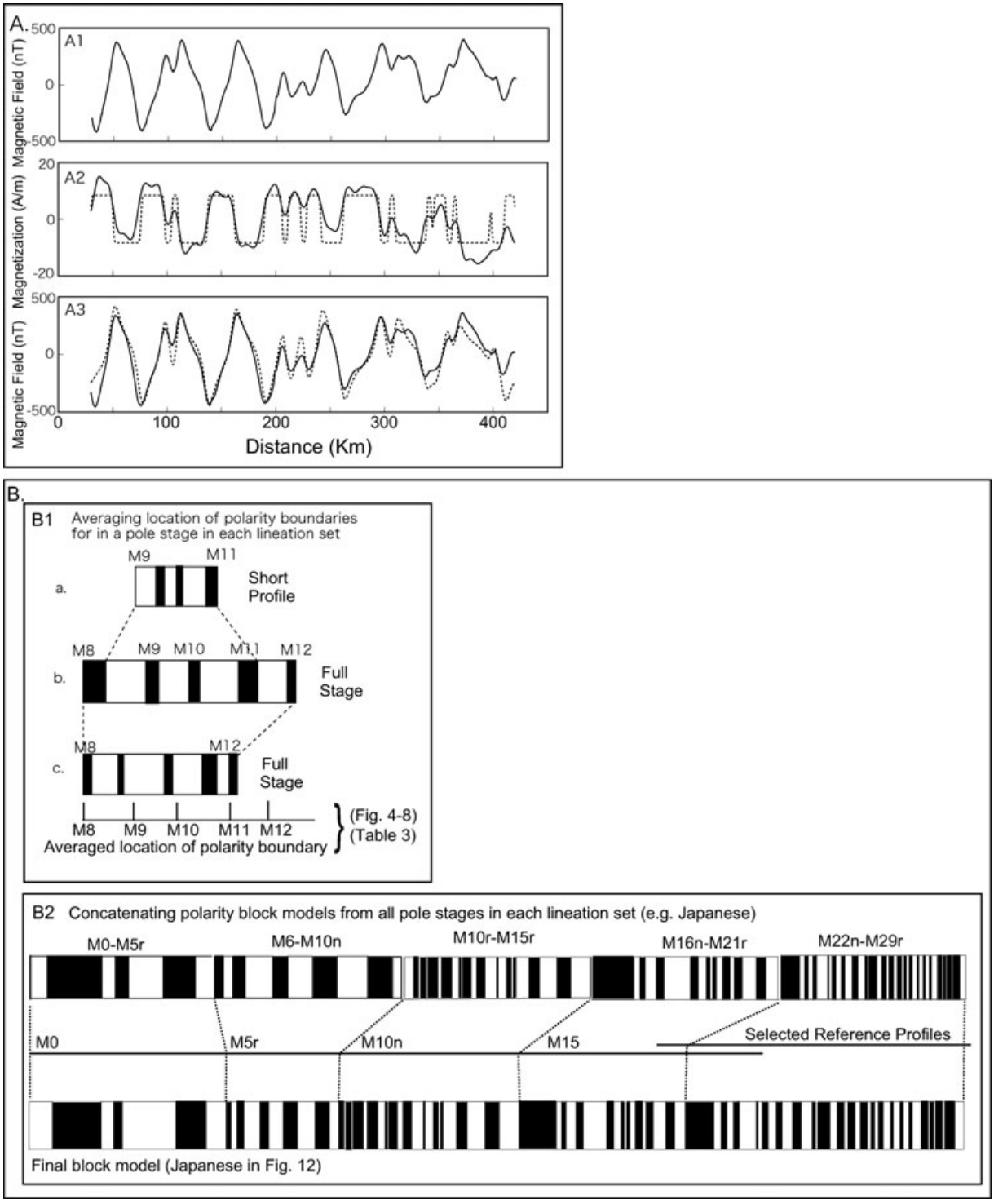

Figure 10. Sketch of the magnetic modelling process. (A1) Observed magnetic anomaly profile (P9, skewed). (A2) Solid line shows inverse results, magnetization values (deskewed). The apparent difference between this magnetization and the original magnetic profile is largely due to anomaly phase shift (skewness). Dotted line shows a polarity block model for the forward model. The polarity block model was Gaussian filtered at polarity boundaries to make finite width polarity transitions. (A3) Solid line shows observed magnetic anomaly profile (same as A1) and dotted line shows calculated anomaly from the polarity block model created in A2. (B1–B2) Normalization process is schematically described (see the details in text). (B1) Blocks a–c represent polarity block models for three individual magnetic profiles. These are normalized to the width of the age group in anomaly number. Model a shows how profile covering less than entire anomaly group is handled. (B2) Polarity blocks for each age group are assembled to make a complete sequence for each lineation set using reference lines (Section 2.4).

Table 2. Widths of modeled polarity chrons (normalized).

Chron	Hawaii	Japanese	Phoenix	Comp.	Age	No.
M0r R	0.00	0.00		0.00	124.16	1
M1n N	2.61	1.79		2.49	125.00	2
M1r (M1) R	10.42	6.77	0.00	9.73	127.46	3
M3n (M2) N	11.94	7.82	0.65	10.83	127.83	4
M3r (M3) R	13.55	9.16	1.69	12.15	128.28	5
M5n (M4) N	18.24	13.09	4.97	16.06	129.60	6
M5r (M5)	21.00	16.77	6.95	18.88	130.56	7
M6n	22.27	18.47	8.64	20.34	131.06	8
M6r	22.63	18.95	9.28	20.79	131.21	9
M7n	23.01	19.48	9.91	21.26	131.37	10
M7r	23.43	20.12	10.72	21.82	131.56	11
M8n	24.74	21.54	12.55	23.21	132.03	12
M8r	25.24	22.39	13.91	23.99	132.29	13
M9n	26.05	23.62	15.29	25.03	132.65	14
M9r	26.82	24.98	16.52	26.08	133.00	15
M10n	27.90	26.66	17.88	27.40	133.45	16
M10r	28.74	27.88	19.04	28.41	133.79	17
M10n1	29.66	28.76	19.88	29.25	134.08	18
M10r1	30.24	29.35	20.86	29.89	134.29	19
M10n2	30.48	29.61	21.10	30.13	134.37	20
M10r2	31.03	30.03	21.91	30.65	134.55	21
M10n3	31.34	30.21	22.14	30.88	134.63	22
M10KNr	31.92	30.87	22.48	31.42	134.81	23
M11n	33.02	31.54	23.24	32.23	135.09	24
M11r	34.78	32.62	23.67	33.39	135.48	25
M11an	35.84	33.49	24.53	34.29	135.79	26
M11ar	36.36	33.82	24.60	34.62	135.90	27
M12n1	37.81	34.06	25.52	35.44	136.18	28
M12r1	39.05	34.95	25.55	36.25	136.45	29
M12n2	39.59	35.43	25.85	36.70	136.60	30
M12r2	40.06	35.77	26.21	37.08	136.73	31
M12n3	41.92	36.89	27.92	38.54	137.23	32
M12r3	42.23	37.20	28.04	38.79	137.31	33
M13Kn	42.88	37.93	28.57	39.42	137.53	34
M13Kr	43.66	38.44	29.46	40.08	137.75	35
M13n	44.08	38.84	29.67	40.44	137.87	36
M13r	44.70	39.15	30.43	40.94	138.04	37
M14n	45.76	40.40	31.33	41.98	138.40	38
M14r	46.18	40.96	31.97	42.48	138.57	39
M15n	47.84	43.04	33.20	44.14	139.13	40
M15r	49.27	44.28	33.47	45.21	139.49	41
M16n	50.23	46.38	34.38	46.54	139.94	42
M16r-e	53.76	52.36	37.37	50.74	141.37	43
M16n-e	54.10	53.14	37.58	51.21	141.52	44
M16r	55.01	53.72	38.02	51.86	141.75	45
M17n	56.83	55.60	39.61	53.57	142.32	46
M17r	58.13	56.69	41.04	54.75	142.73	47
M18n	62.39	60.42	46.73	58.90	144.13	48
M18r	64.27	61.53	48.53	60.38	144.64	49
M19n1	66.56	62.85	50.06	62.04	145.20	50
M19r1	67.26	63.22	51.42	62.71	145.43	51
M19n2	68.12	63.44	51.91	63.21	145.60	52
M19r2	71.09	64.57	52.73	64.92	146.18	53
M20n1	71.67	65.49	53.54	65.65	146.42	54
M20r1	72.91	67.01	54.86	66.95	146.87	55
M20n	73.36	67.52	55.33	67.41	147.02	56
M20r	75.74	68.15	56.18	68.71	147.46	57
M21n	78.33	69.90	58.55	70.82	148.18	58
M21r	80.10	71.49	60.00	72.37	148.70	59
M22n1	81.57	73.15	61.77	73.90	149.22	60
M22r1	83.17	75.81	65.39	76.24	150.01	61
M22n2	83.36	76.61	65.66	76.66	150.16	62
M22r2	83.95	77.18	66.58	77.28	150.37	63
M22n3	84.12	77.78	66.97	77.65	150.50	64
M22r3	84.32	78.07	67.65	77.97	150.60	65
M22 An	85.65	80.05	70.92	79.87	151.25	66
M22Ar	85.76	80.36	72.18	80.28	151.39	67
M23n	86.33	80.80	73.72	80.96	151.62	68
M23r1r	86.79	81.54	75.59	81.79	151.90	69
M23r1n	87.22	82.12	76.14	82.28	152.06	70
M23r2r	87.38	82.55	76.73	82.62	152.18	71
M24n	88.34	83.45	78.59	83.69	152.54	72
M24r	88.67	84.30	79.71	84.36	152.77	73
M24An	89.20	85.39	81.00	85.23	153.06	74
M24Ar	89.33	85.84	81.28	85.50	153.16	75
M24Bn	89.81	86.60	82.38	86.19	153.39	76
M24Br	90.09	87.27	83.35	86.74	153.58	77
M25n	90.49	87.92	84.46	87.36	153.79	78
M25r	91.09	88.54	86.26	88.17	154.06	79
M25n2	91.26	89.10	86.57	88.51	154.18	80
M25r2	91.62	89.63	87.49	89.03	154.35	81
M25n3	92.08	90.29	89.35	89.82	154.62	82
M25r3	92.41	90.88	89.95	90.29	154.78	83
M25n4	92.75	91.24	90.49	90.66	154.91	84
M25r4	92.94	91.79	91.75	91.19	155.09	85
M25n5	93.27	92.19	92.53	91.62	155.23	86
M25r5	93.53	92.44	93.17	91.93	155.34	87
M26n	93.93	92.99	94.34	92.53	155.54	88
M26r	94.70	93.08	95.10	93.00	155.70	89
M27n	94.88	93.63	96.49	93.55	155.83	90
M27r	95.25	94.10	96.89	93.95	156.04	91
M28n	95.65	94.68	98.12	94.56	156.22	92
M28r	95.97	95.15	99.18	95.07	156.45	93
M28Kn	96.55	96.00	100.00	95.78	156.59	94
M28Kr	96.71	96.56		96.19	156.76	95
M28K2n	97.32	96.80		96.66	156.90	96
M28K2r	97.71	97.15		97.08	157.05	97
M28K3n	98.33	97.34		97.54	157.21	98
M28K3r	98.44	98.04		98.01	157.35	99
M29n	98.99	98.22		98.42	157.63	100
M29r	99.41	99.27		99.25	157.89	101
	(100)	(100)		(100)		(102)

the M-anomaly model has similar precision as that well-accepted C-anomaly timescale.

4 DISCUSSION

4.1 What is the 'Representative' polarity block sequence for a timescale?

In previous studies, polarity block modelling was carried out with a small number of profiles and focused on one lineation set (Hawaiian). That restriction can be problematic because each individual magnetic profile contains perturbations caused by geologic 'noise', that is irregularities in the anomaly spacing and shapes resulting from the crustal recording process and tectonic complications. For example, even in the Hawaiian lineation set where M-anomaly lineations have been well identified within multiple continuous profiles (e.g. NOAA1–4 in Table 1), we do not know which profile is the 'best' one. This is clear when comparing two composite polarity block models: the one scaled to a single reference profile (e.g. NOAA4, the approach used in CENT95) and the other scaled to the averaged Hawaiian reference profile (Fig. 12). Comparing these two models, however, shifts of polarity boundary

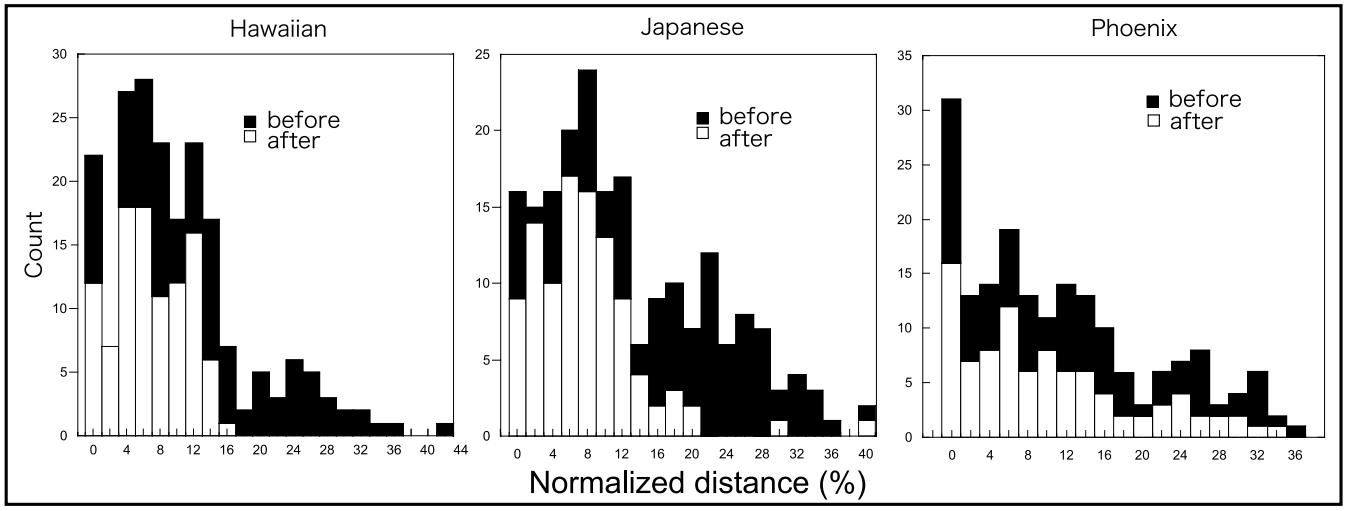

Figure 11. The distribution of standard deviations of individual polarity block boundaries. Black columns show deviations before and white columns show after the outlier rejection process was applied (Section 2.4). Vertical axis indicates the number of count. Horizontal axis indicates standard deviation of polarity block models expressed by normalized distance (per cent) relative to the anomaly age group. Standard deviations in kilometres are given in Table 3.

locations are observed, indicating that the selection of one 'representative' profile is a poor approach for the construction of an objective timescale model. For another example of the difficulty of choosing a representative M-anomaly profile, we note the variability of the Phoenix lineations. These lineations suggest a complicated tectonic environment in the Nauru Basin and central Pacific basin near Magellan Rise, an area that includes many ridge jumps and fracture zones (Nakanishi *et al.* 1992). In this area, one can find that the length of M5–M10 varies by a factor of two among different spreading segments (see Fig. 19 in Nakanishi *et al.* 1992). Without external age control, it is almost impossible to determine which spreading rate is the best representation and thus which anomaly profile is the best reference.

A more representative model can be derived by averaging many profiles covering a wide geographic area. Such a model is an improvement for two reasons: (1) averaging many, selected anomaly profiles improves the fidelity of the composite because random variations in anomaly spacing, shapes, and amplitudes are averaged out and (2) wide geographic spacing insures that the magnetic changes are global in nature and errors caused by local tectonic factors, such as ridge jumps or spreading rate changes can be recognized and excluded. Our use of 87 magnetic anomaly profile segments, representing each of the five age groups with an average of 18 profiles, is a factor two larger than the data set used for the widely accepted C-anomaly GPTS (Cande & Kent 1992a). This redundancy has allowed us to determine the location of polarity boundaries with a precision comparable with that study.

4.2 M-anomaly correlation

We observed a high degree of correlation among anomalies in each of the three lineation sets for the M0–M24 anomalies, as indicated by mostly small standard deviations in the location of polarity boundaries. The general lack of significant differences between our model and previous versions implies that the recording of magnetic anomalies by the Pacific Plate ridges during this time period was remarkably regular.

The correlation of the M25–M29 anomalies in the sequence is a special problem. Although we can correlate anomalies consistent with previously defined M25–M29, there is larger variability, as compared to M0–M24 correlations, and the variability can be attributed to less accurate location of polarity boundaries within the closely spaced, short-wavelength, low-amplitude anomalies. With the difference in characteristics between the M25–M29 and M0–M24 correlatability, we ask two questions: (1) do M25–M29 anomalies represent actual polarity reversals? and (2) even if the M26-M29 anomalies are attributed to polarity reversals, do we extend the GPTS based on the correlation of these less consistent anomalies?

The M26–M29 anomalies were previously examined on 13 profiles in the three lineation sets across the western Pacific (Cande *et al.* 1978). The number and spacing of these small anomalies were found to be consistent, but the anomaly amplitudes are much smaller than that of younger anomalies (Figs 4–8). Cande *et al.* (1978) discussed the origin of these anomalies and whether they represent actual short polarity reversals or fluctuations of magnetic field intensity with uniform polarity. The conclusion was that the smooth increases in anomaly amplitude from M29 forward in time connect the M25–M29 anomalies with the M0–M24 anomalies and that they have common origin, which is polarity reversals (Cande *et al.* 1978).

Because of uncertainty about the cause of such small anomalies (Cande & Kent 1992b; Sager *et al.* 1998; Tivey *et al.* 2006; Tominaga *et al.* 2008), it is not certain that all of these anomalies result from polarity reversals. Terrestrial magnetostratigraphy shows many polarity chrons identified within M25–M29 (Ogg & Gutowski 1995; Pryzbyiski & Ogg 2007), but it is challenging to make a one-to-one correlation between polarity reversals in terrestrial magnetostratigraphy and marine magnetic anomalies of this age. At best, we can say that the magnetostratigraphic record shows alternating polarity chrons of the appropriate duration and age, so we suggest that this supports the interpretation of the M25–M29 anomalies as actual polarity reversals.

Although we accept the M25–M29 anomalies as polarity reversals, whether they should contribute to the extension of the GPTS is debatable. Anomalies M0–M29 have been widely identified and the correlations have been well accepted (Cande *et al.* 1978; Nakanishi *et al.* 1989; Nakanishi *et al.* 1992; Channell *et al.* 1995). However,

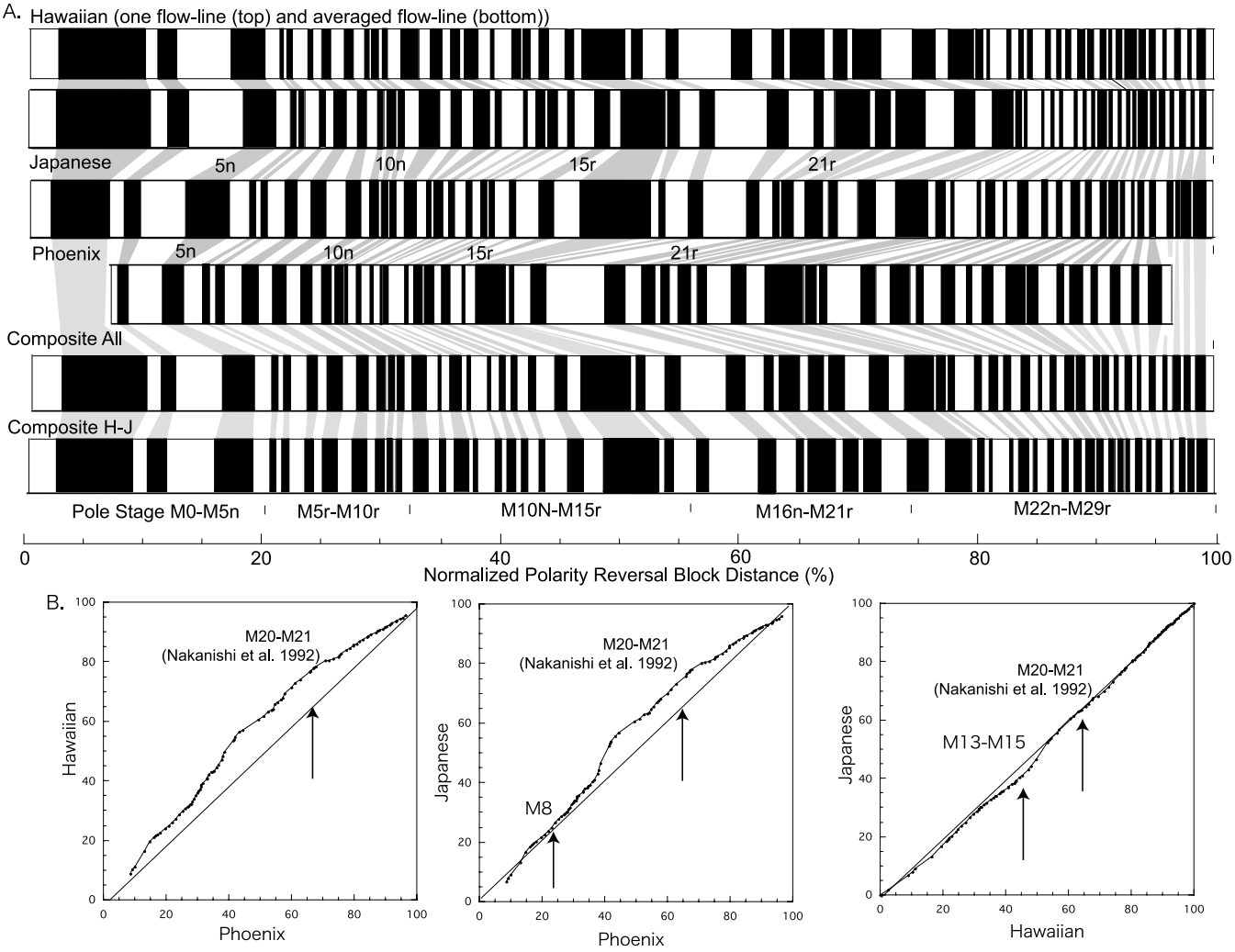

Figure 12. (A) Block models plotted versus normalized distance. Top four sequences are from the Hawaiian, Japanese, and Phoenix lineation sets. Top two block models show difference between a model based on one Hawaiian anomaly profile (upper) and an average of many Hawaiian anomaly profiles. Bottom two sequences are a composite model constructed from all three lineation set models and another that leaves out the Phoenix model. Positive polarity block correlations are indicated with grey shaded bands. The horizontal axis indicates the normalized distance. (B) Comparison of polarity block models between different lineation sets. Both vertical and horizontal axes indicate normalized distance (Table 2). Straight diagonal lines represent (left) Phoenix versus Hawaiian, (middle) Phoenix versus Japanese, and (right) Japanese versus Hawaiian. Arrows denote periods of simultaneous changes in spreading regime (M20–M21 suggested in Nakanishi *et al.* 1992, see text).

because of the small anomaly amplitudes, some anomalies may be geomagnetic field intensity fluctuations rather than reversals (e.g. Bowles *et al.* 2003). Furthermore, owing to the short wavelengths and less distinctive nature of individual anomalies, it is possible that we can miscorrelate some of the anomalies in the M25–M29 period. In this portion of the sequence, the GPTS is not as well founded, and thus should be interpreted and used with some caution. To improve correlations, higher resolution data, such as deep-tow magnetic profiles from a wide geographic area would be useful.

4.3 Identification of subchrons (short duration reversals)

The meaning of small anomalies has been in debate because it is difficult to determine whether those small anomalies represent reversals or not (e.g. Cande & Kent 1992b; Sager *et al.* 1998; Tominaga *et al.* 2008). Cande & Kent (1992a) excluded anomalies with durations of <30 kyr, arguing that these short anomalies are more likely to result from geomagnetic field intensity fluctuations than polarity reversals. However, this value is arbitrary and there is no reliable duration cut-off that we can utilize.

In this study, nearly 60 per cent of the subchrons in our GPTS have a duration >0.2 Ma. Only a few subchrons (M10r1, M10r2, M12.n3), identified in both previous studies and magnetostratigraphy, have durations of <0.1 Ma, and the rest of the subchrons span 0.1–0.3 Ma. These durations are about three orders of magnitude longer than the cut-off value used in Cande & Kent (1992a) suggesting that they are probably due to polarity reversals. For the two 'excursions' suggested in Speranza *et al.* (2005), we include both in our GPTS because they meet our conservative acceptance criteria. One is included for the first time (M16n.1r) and the other was suggested in previous GPTS (M20n.1r). The durations of M16n.1r and M20n.1n are 0.16 and 0.44 Ma, respectively (Table 2). We observe that the anomalies defining these subchrons are no different from other observed correlatable, small anomalies that have been interpreted as reversals.

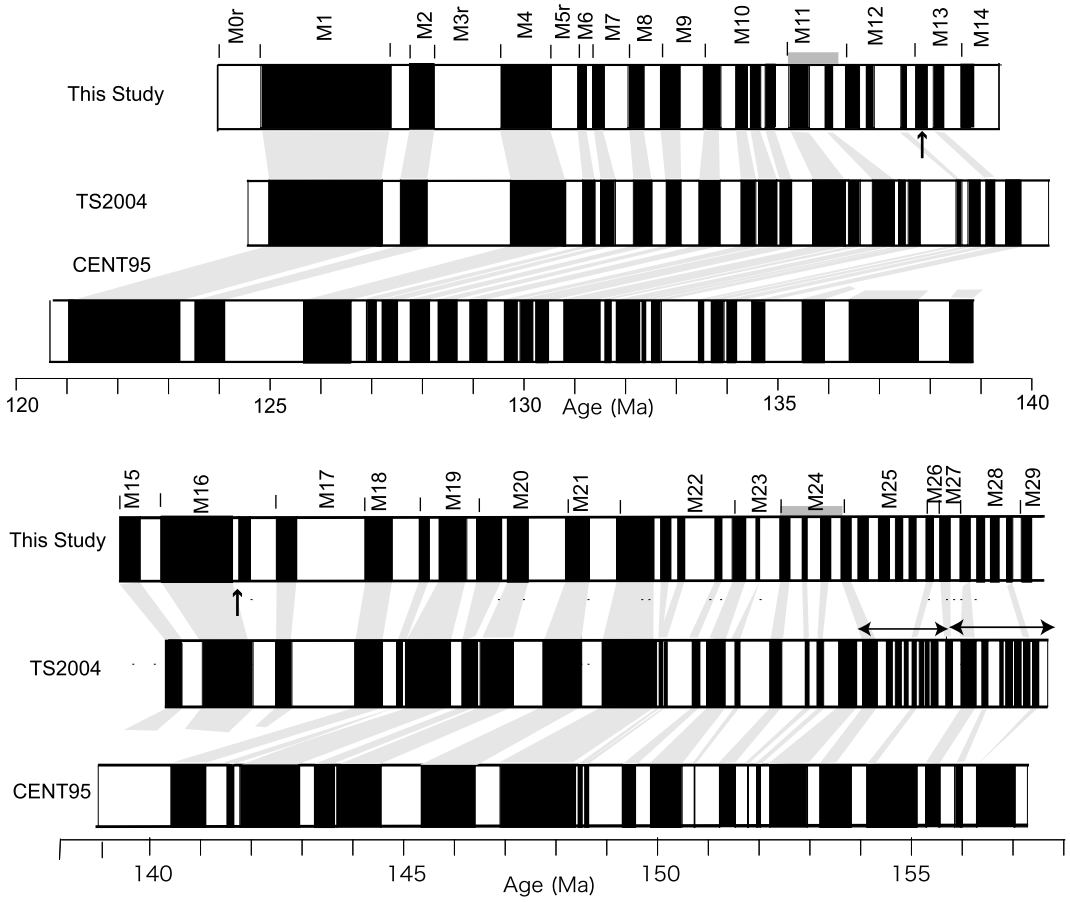

Figure 13. New M-anomaly GPTS and comparison with the CENT95 (Channell *et al.* 1995) and TS2004 (Gradstein *et al.* 2005) models. 'This study' is the composite model from all the three Pacific lineation sets. Arrows show correlations where two new subchrons were added (in M13 and M16). Grey bands next to the new GPTS show locations where subchrons were dropped (in M11 and M24). Note that CENT95 did not include subchrons in pre-M25 anomalies and had additional subchron in M24. Arrows over M25–M29 in TS2004 indicate that the TS2004 model used different reference block models for M0–M24 (Larson and Hilde 1975), M25–M27 (Handshumacher *et al.* 1988) and pre-M28 (Sager *et al.* 1998). In particular, the larger numbers of subchrons in M25–M29 are derived from aeromagnetic (Handshumacher *et al.* 1988) and deep-towed magnetic (Sager *et al.* 1998) data.

4.4 Changes in spreading rates

It is important to examine the implications of our GPTS construction methodology for changes in seafloor spreading that affect the GPTS. Cande & Kent (1992a) applied their C-anomaly GPTS, which was calibrated from anomalies recorded at a single ridge, to investigate Cenozoic seafloor spreading history on several ridges in different oceans. They reasoned that the optimal GPTS would minimize apparent abrupt changes in seafloor spreading when applied to a global array of spreading ridges. A similar approach would be sensible for the M-anomaly GPTS, but cannot easily be accomplished for two reasons. One is that sparse age constraints for the M-anomaly GPTS leave us little choice in adjusting the anomaly sequence because we can only interpolate ages between two dates, one on each end of the sequence. The other is that the Pacific M-anomalies are the only well defined, complete sequence in which all anomalies are clearly identified, so comparison with other oceans is difficult. Nevertheless, we can investigate possible spreading rate variations within Pacific Plate by comparing the three lineation sets.

To understand implications about spreading rates, it is helpful to review how such rates were treated in the polarity sequence model construction. For most steps of the analysis, spreading rates were removed as a factor by normalization. This step translated the anomaly sequence from distance in kilometers to a unit-less distance (i.e. percent of total). Anomaly age groups were combined into whole lineation set models and a composite model (Fig. 12). The polarity block lengths from the five age groups were adjusted in proportion based on the spacing of endpoint anomalies for the age groups in reference profiles. There is, however, a subtle assumption about spreading rates in this method: we have tacitly assumed that each anomaly occupies the same percentage of a given sequence on each ridge. In essence, this means that the ratio of spreading rates among the three ridges remained constant. This seems a reasonable first-order assumption because spreading rates in many oceans appear to change little for long periods between major tectonic reorganizations. Furthermore, without independent evidence of changes in the spreading rate ratios among the three ridge systems, it is difficult to make a more accurate assumption.

To further investigate differences in spreading rate among the three ridge systems, we plot, one-to-one, the polarity duration from pairs of the three lineation sets (Fig. 12B). If each of the two compared lineation sets maintained a constant spreading rate through the M0–M29 time period, the polarity block comparison curve should form a straight line. Departure from a straight line indicates differences in percentage spreading rates. This is because for constant spreading the width of a polarity block (or group of polarity blocks) in all three lineation sets should occupy same percentage of the M0–M29 time period.

Table 3. Standard deviations of polarity model chron boundaries (km).

Chron	Hawaii	*N*	Japanese	*N*	Phoenix	*N*	Composite	Total *N*
M0r	7.26	3/3	19.43	3/3			13.34	6
M1n	10.06	5/5	36.51	3/3			23.29	7
M1r	19.15	5/7	30.99	3/4	1.11	3/3	17.08	11
M3n	16.57	6/7	10.15	4/4	4.28	3/3	10.33	13
M3r	8.49	5/7	6.19	5/6	1.84	3/4	5.51	13
M5n	0.79	5/7	1.76	5/6	0.64	4/4	1.06	14
M5r	4.64	6/6	7.06	8/8	2.31	3/3	4.67	17
M6n	4.92	4/6	4.36	5/8	1.56	3/3	3.61	12
M6r	6.01	4/6	4.52	7/8	2.79	3/4	4.44	14
M7n	7.22	4/6	4.09	5/8	2.44	4/4	4.58	13
M7r	5.48	4/6	0.74	5/8	3.61	4/4	3.28	13
M8n	6.71	5/6	3.82	4/9	5.42	3/4	5.32	12
M8r	5.73	4/5	5.20	4/9	7.00	4/4	5.97	12
M9n	5.04	4/5	5.07	5/9	4.46	3/4	4.86	12
M9r	2.05	4/5	3.14	7/9	4.05	3/4	3.08	14
M10n	2.34	4/5	0.59	5/9	0.52	4/4	1.15	13
M10r	11.60	3/3	2.81	4/4	0.00	1/1	4.80	8
M10Nn.1n	9.55	3/3	6.67	4/4	0.00	1/1	5.41	8
M10Nn.1r	10.80	3/3	5.66	4/4	0.00	1/1	5.49	8
M10Nn.2n	11.77	3/3	9.54	3/4	0.00	1/1	7.10	7
M10Nn.2r	12.02	3/3	11.97	4/4	0.00	1/1	8.00	8
M10Nn.3n	11.83	3/3	10.87	4/4	0.00	1/1	7.56	8
M10Nr	11.35	3/3	14.85	4/6	0.00	1/1	8.73	8
M11n	12.03	4/4	13.93	4/6	3.07	2/2	9.68	10
M11r	14.74	3/3	16.12	4/6	6.84	2/2	12.57	9
M11An	18.88	3/3	16.25	3/6	6.39	2/2	13.84	8
M11Ar	27.79	2/3	21.32	3/6	4.22	2/2	17.78	7
M12n	22.50	3/4	22.18	5/6	1.34	2/3	15.34	10
M12r.1r	25.20	3/4	20.89	5/8	1.99	2/2	16.03	10
M12r.1n	23.68	3/4	20.88	5/8	0.36	2/2	14.97	10
M12r.2r	21.10	2/4	19.34	5/8	4.82	2/2	15.09	9
M12An	22.11	3/4	20.79	6/8	5.28	2/2	16.06	11
M12Ar	21.00	3/4	20.32	6/8	3.20	2/2	14.84	11
M13n.1n	25.77	3/4	19.94	6/8	4.76	3/3	16.82	12
M13n.1r	19.74	2/3	22.09	2/6	2.76	3/3	14.86	7
M13n.2n	18.18	2/5	14.97	3/6	2.26	4/4	11.80	9
M13r	20.25	4/5	16.52	7/9	1.88	4/4	12.88	15
M14n	19.54	3/5	11.69	5/9	3.56	4/4	11.60	12
M14r	18.67	4/5	13.28	7/9	3.39	4/4	11.78	15
M15n	16.48	3/5	20.28	6/7	1.63	4/4	12.80	13
M15r	17.41	4/5	8.18	4/7	2.80	4/4	9.46	12
M16n	12.67	6/6	0.00	1/1	9.44	3/3	7.37	10
M16n.1r	13.37	4/6	0.00	1/1	9.32	3/3	7.56	8
M16n.2n	12.88	5/6	0.00	1/1	7.66	3/3	6.84	9
M16r	22.22	5/6	0.00	1/1	4.24	3/3	8.82	9
M17n	23.06	5/7	7.22	3/3	5.86	5/5	12.04	13
M17r	36.00	4/7	3.02	3/3	10.11	5/5	16.38	12
M18n	26.60	4/7	4.19	4/4	8.55	5/5	13.11	13
M18r	20.71	4/7	5.77	4/4	4.74	5/5	10.41	13
M19n.1n	14.41	4/5	2.98	4/4	5.83	5/5	7.74	13
M19n.1r	11.95	4/4	3.57	3/3	4.23	3/3	6.58	10
M19n.2n	16.79	3/4	20.81	3/3	1.17	3/3	12.92	9
M19r	17.12	3/4	16.34	3/3	1.13	3/3	11.53	9
M20n.1n	18.68	3/6	27.04	3/3	0.00	3/3	15.24	9
M20n.1r	19.34	3/6	25.18	3/3	0.00	1/1	14.84	7
M20n.2n	23.70	4/6	20.66	3/3	0.00	1/1	14.79	8
M20r	28.60	4/6	11.68	3/3	9.89	3/3	16.72	10
M21n	17.58	4/5	1.10	3/3	18.77	3/3	12.48	10
M21r	13.51	3/5	0.15	3/3	23.87	2/2	12.51	8
M22n.1n	0.00	1/1	17.37	6/6	28.96	2/2	15.45	9
M22n.1r	0.00	1/1	14.78	4/6	30.75	2/2	15.18	7
M22n.2n	0.00	1/1	12.30	4/6	27.92	2/2	13.40	7
M22n.2r	0.00	1/1	11.24	4/6	29.88	2/2	13.71	7
M22n.3n	0.00	1/1	9.64	4/6	24.36	2/2	11.33	7

Table 3. (*Continued.*)

Chron	Hawaii	*N*	Japanese	*N*	Phoenix	*N*	Composite	Total *N*
M22r	0.00	1/1	16.39	4/6	28.45	2/2	14.95	7
M22An	0.00	1/1	17.93	6/6	33.24	2/2	17.06	9
M22Ar	0.01	1/1	16.65	5/6	25.95	2/2	14.20	8
M23n	5.19	4/4	18.20	7/8	21.14	3/3	14.84	14
M23r.1r	2.39	4/4	17.70	7/8	23.53	3/3	14.54	14
M23r.1n	2.66	4/4	15.64	7/8	22.56	3/3	13.62	14
M23r.2r	2.69	4/4	9.54	5/8	23.51	3/3	11.91	12
M24n	3.67	4/4	11.67	5/9	23.06	3/3	12.80	12
M24r.1r	2.62	4/4	12.93	5/9	19.80	3/3	11.79	12
M24r.1n	2.83	3/4	14.13	3/9	21.06	3/3	12.67	9
M24r.2r	3.82	3/4	16.69	6/9	15.99	3/3	12.17	12
M24An	4.27	3/4	17.74	6/9	16.17	3/3	12.73	12
M24Ar	4.81	4/4	18.48	5/9	14.91	3/3	12.73	12
M25n	5.91	4/4	20.68	6/9	13.41	3/3	13.33	13
M25r	4.78	4/4	24.45	5/8	12.62	3/3	13.95	12
M25An.1n	5.58	4/4	24.67	6/8	13.38	3/3	14.55	13
M25An.1r	5.89	4/4	26.90	5/8	11.83	3/3	14.87	12
M25An.2n	5.92	4/4	25.42	6/8	15.71	3/3	15.68	13
M25An.2r	7.80	4/4	25.90	5/8	14.55	3/3	16.08	12
M25An.3n	7.84	4/4	24.43	5/8	10.31	3/3	14.20	12
M25Ar	7.38	4/4	24.85	6/8	11.54	3/3	14.59	13
M25n5	9.61	4/4	25.09	7/8	10.33	3/3	15.01	14
M25r5	7.60	4/4	8.88	6/8	4.10	3/3	6.86	13
M26n	9.05	3/3	7.11	3/8	6.26	3/3	7.47	9
M26r	7.51	3/3	7.89	6/8	2.47	3/3	5.95	12
M27n	10.95	3/3	9.84	3/6	3.58	3/3	8.12	9
M27r	4.16	3/3	12.51	4/6	0.09	3/3	5.58	10
M28n	8.13	3/3	12.17	4/6	0.00	3/3	6.77	10
M28r	4.67	3/3	5.57	4/6		1/1	5.12	8
M28An	7.92	3/3	14.36	4/6			11.14	7
M28Ar	4.47	3/3	13.01	2/2			8.74	5
M28Bn	4.34	2/3	16.77	2/2			10.55	4
M28Br	3.00	2/3	15.04	2/2			9.02	4
M28Cn	3.11	2/3	20.31	2/2			11.71	4
M28Cr	0.12	2/3	19.82	2/2			9.97	4
M29n	7.61	2/3	21.96	2/2			14.78	4
M29r	10.05	2/3	20.94	2/2			15.49	4

N, number of polarity boundaries used for averaged polarity block model (left of /) and collected segments from profiles in Table 1 (right of /). These standard deviations were referenced to distance along the following magnetic profiles: Hawaiian, NOAA1–4; Japanese, V2006, V2110, C1219, DSDP32, V3212, GH7901 and GH805; Phoenix, V3401, V3214, C1205, NOVA1AHO and C1304.

The relative percentage spreading curves (Fig. 12B) show that the Japanese and Hawaii anomalies relative to the Phoenix anomalies appear similar, indicating that spreading ridges recorded the Japanese and Hawaiian lineations nearby identically. Going forward in time, from M29 to about M20 to M21, both Hawaiian and Japanese lineations develop an offset of ∼10 per cent relative to the Phoenix lineations. This implies that these anomalies occupy a greater percentage of the entire sequence for the Phoenix lineations (∼25–30 per cent) than for the other lineation groups (∼20 per cent). From M20 to M21 to about M10N, the percentage spreading curves are parallel, implying that these anomalies take up the same space in all three lineation groups. Finally, from M10N to M0, the offset between the Hawaiian and Japanese lienations relative to the Phoenix lineations diminishes as this portion of the sequence represents a greater proportion for the Hawaiian and Japanese lineations (∼53 per cent) as compared with the Phoenix lineations (∼43 per cent).

Although differences in spreading regime are observed among the three ridge systems, the differences are not large and the models are mostly consistent, especially between the Japanese and Hawaiian anomalies. Without independent data to determine and correct for actual spreading rates, our composite model is a reasonable approximation of the overall anomaly sequence. Despite these observed differences in spreading, we think that our composite model is a better representation of the polarity sequence than previous models that were based on one ridge system, because ours is a wide-area average.

4.5 Comparison to previous polarity block models

In Fig. 13, polarity block GPTS models from previous studies are compared with our Pacific composite model. The overall time span of the composite M-anomaly GPTS is shorter than that of CENT95 and TS2004 because of the older age that we used for the base of M0r (Channell *et al.* 2000; Gradstein *et al.* 2005) (Fig. 13). The shorter M0–M29 time period makes the frequency of reversals slightly higher, especially in M21–M29, as compared to the reversal frequency in the same anomalies reversals in CENT95 and TS2004.

Our composite GPTS model shows minor differences in the distribution of polarity reversals compared to previous studies. The polarity sequences in CENT95 and TS2004 are almost the same, particularly for M0–M24, presumably because both are based primarily on the NOAA magnetic profiles from the Hawaiian lineation set. For pre-M24 reversals, CENT95 and TS2004 are significantly different because CENT95 did not identify any subchrons in M25. In contrast, TS2004 used M25 and older polarity chrons derived from aeromagnetic and deep-tow magnetic data with higher resolution than the sea surface data used for other chrons. Comparing our GPTS to the previous studies, the distributions of polarity reversals within M0–M10 and M12–M21 are about the same, and M11–M12 and M22–M29 are similar but the polarity seems to be biased towards normal in previous models whereas the polarity seems to be distributed more-or-less equally in our model. This difference between our model and the previous model is because our model is based on magnetic profiles from all the Pacific lineation sets (Hawaiian, Japanese and Phoenix) whereas previous GPTS models were based only on a few Hawaiian magnetic profiles that have more normal polarity in these anomalies.

4.6 Age calibration

A significant challenge for the current M-anomaly GPTS is age calibration, which is poor owing to the paucity of reliable radiometric dates directly tied to magnetic anomalies. Unlike Cande & Kent (1992a), who could use nine radiometric ages for calibration, we found only two dates that seem reasonably well constrained for our GPTS: 125.0 Ma for M0 and 155.7 Ma for M26. The former date is suggested from a recent revision of the Aptian/Barremian stage boundary (Channell *et al.* 2000) and reevaluation of biostratigraphy and radiometric age data from MIT Guyot in the Pacific (Pringle *et al.* 2003; Gradstein *et al.* 2005). The latter date is from $^{40}Ar/^{39}Ar$ dating of celadonite veins cored from M26-age crust in the Argo Abyssal plain (Ludden 1992). Although there may have been a time lag because celadonite was deposited by hydrothermal processes, it is thought that the delay was small because the hydrothermal circulation was likely driven by heat near the ridge crest. Unlike TS2004, we did not use stratigraphic stage boundary ages because they are indirect and include uncertainty in the determination of stage boundary ages in terrestrial stratigraphy and their correlation to the reversal sequence.

The age of the base M0r (base-Aptian) is still in a debate (Channell *et al.* 2000; Chambers *et al.* 2004; Gong *et al.* 2008; He *et al.* 2008). TS2004 used an age of 125 Ma derived by $^{40}Ar/^{39}Ar$ dating of samples cored from MIT Guyot for the base of M0r because this date is correlated to the marine fossil record that is generally used to determine a global strato-type. A recent study using $^{40}Ar/^{39}Ar$ dating of basalt outcrops in China suggests that possible M0r layers are dated at ∼121 Ma (He *et al.* 2008). This younger M0r age is used in a series of tectonic studies on the north Atlantic ocean and related orogeny (e.g. Srivastava *et al.* 2000; Sibuet *et al.* 2004; Fiet *et al.* 2006). However, further confirmation for the younger M0r age by He *et al.* (2008) is necessary because (1) the reversed polarity sites are not confirmed as being within M0r because they are isolated and not in the context of other polarity zones, and (2) there is no correlation to the marine fossil record that defines stratigraphic stages. Other recent stratigraphic studies support an older age for M0. A new U-Pb age for the Aptian-Albian boundary of 112 Ma (Selby *et al.* 2009) and a cycle-stratigraphy study suggests that the duration of the Aptian stage is ∼13 Myr (Huang *et al.* 2009). Together, these data support a base-Aptian (M0r) age of about 125 Ma. Because this is consistent with the $^{40}Ar/^{39}Ar$ date from the MIT Guyot and the current global strato-type suggested by Channell *et al.* (2000), we use 125 Ma for the age of the older boundary of M0r.

There are other dates available in between M0 and M29, but none are direct or free of uncertainty. Many available dates of basement from drilled cores on the M-anomalies are biostratigraphically derived and lack the accuracy of radiometric ages (e.g. DSDP Site 417 (M0r) in the Atlantic, DSDP Site 303 (M4), 304 (M9) and 307 (M21) in the Pacific). A couple of radiometric ages measured on basement cores drilled on M-anomalies are not used in this study. One is the Ar^{40}/Ar^{39} date (126 Ma) from basalt core at DSDP Site 387 in the Atlantic for M16. This date is significantly offset from biostratigraphic ages from overlying sediments. Furthermore, this date is close to the accepted age of M0. For both reasons, this date is probably misleading. The other is a 127 Ma Ar^{40}/Ar^{39} date from a basalt core drilled at ODP Hole 1149D on anomaly M12 in the western Pacific M12 (Koppers *et al.* 2003). This age is also significantly younger than expected on the basis of TS2004 age for the M12 anomaly. Moreover, older (132 Ma) nannofossils are found in the basal sediments, suggesting that the cored igneous rocks may be late stage sills above the basement.

Without a larger series of age calibration points, uncertainty in the absolute duration of each polarity block in our model remains greater than other well calibrated GPTS (e.g. Quaternary in TS2004, Gradstein *et al.* 2005). Although absolute ages remain poorly defined, the polarity reversal sequence is robust and can be recalibrated when more reliable ages become available.

4.7 Implication of the new M-anomaly GPTS

Differences between our GPTS and previous models are first explained by differences in the collection of magnetic profiles and the particulars of age calibration points. Both CENT95 and TS2004 are based on a small number of magnetic profiles from the Hawaiian lineations, so they contain information from only a small portion of the Pacific M-anomalies. The GPTS developed in this study is an average representation of many magnetic profiles with wide geographic distribution.

The distribution of polarity reversals affects polarity reversal rates, which have been used to investigate paleogeomagnetic field behaviour. Although reversal rate curves derived from CENT95, TS2004 and this study are similar, our study gives a slightly smoother curve compared to other two (Fig. 14). The CENT95 curve shows a peak in reversal rates between 130.0 and 135.0 Ma and diminishing rates before 150.0 Ma. The peak is attributed to many subchrons between M10 and M15, and the pre-150 Ma decline is attributed to omitted subchrons in the pre-M24 reversal sequence. The TS2004 curve also has a peak between 135.0 and 140.0, but it shows an abrupt increase to high rates between 152.0 and 157.0 Ma. Again the young peak results from M10 to M15 subchrons. This peak is offset from CENT95 because of an older age used for M0. The abrupt pre-150 Ma peak is attributed to the discontinuity resulting from the use of polarity block models made from higher resolution magnetic profiles in Handshmacher *et al.* (1988) and Sager *et al.* (1998). The curve from this study is similar to that from TS2004, but it is smoother and does not show such an abrupt rise before M25. This smoothness results from the more even distribution of polarity blocks as compared to the other two models and it implies that changes in reversal rate were smoother than previous models. If one accepts the premise that actual changes

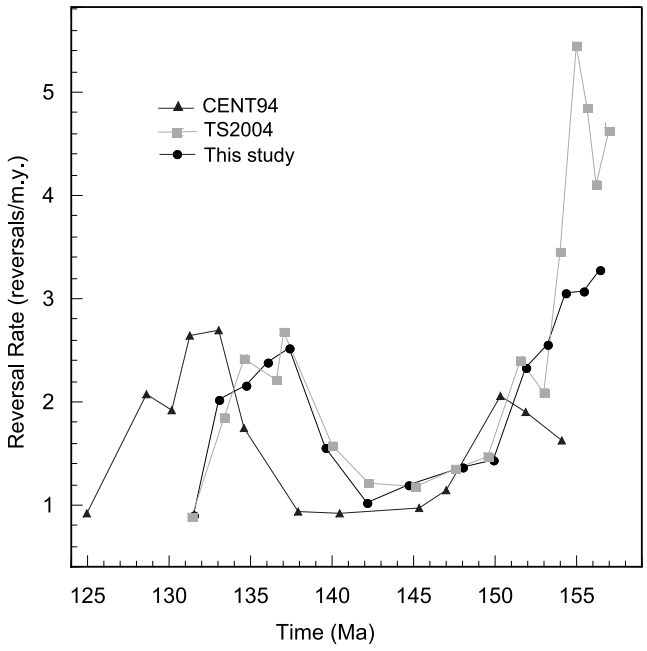

Figure 14. Late Jurassic–Early Cretaceous magnetic polarity reversal rate versus age for the GPTS calculated in this study compared with others. Reversal rate values were calculated at 2 Myr intervals with a 4 m.y. sliding window. Note that the CENT95 timescale has an offset at M0 compared to TS 2004 and this study that is a result of a younger age assignment for M0.

in reversal rate were more likely to have been smooth, then this observation implies that our model is a better representation of the polarity sequence.

4.8 Atlantic M-anomalies

It is natural to compare M-anomalies observed elsewhere in the ocean basins with the new Pacific composite GPTS model. Most extra-Pacific M-anomaly sequences are incomplete and difficult to correlate, but the North Atlantic M-anomalies contain a complete sequence from M0 to M25. Older anomalies are not widely recognized in the North Atlantic because of their low amplitudes (Figs 15A and B).

4.8.1 Keathley and canary block models

We constructed an Atlantic M-anomaly block model in a manner similar to the Pacific models. We used a total of four anomaly profiles from the Keathley lineations (off northeast coast of the United States) and seven from the Canary lineations (off northwest coast of Africa). All profiles are located between the Atlantis and Kane fracture zones (Appendix A). These profiles are closely spaced and perpendicular to the previously determined lineation strikes, and because they contain the entire anomaly sequence, we did not have to normalize the profiles; instead, we used actual distance to calculate polarity spacing. To deskew the magnetic anomaly profiles, we used paleoinclination and paleodeclination determined from average paleomagnetic poles for North America (120, 130, 140 and 150 Ma from Besse & Coutillot 2002).

The north Atlantic polarity model has standard deviations of polarity boundary locations (4–28 km) similar to the Pacific model through M0–M5r and M16n–M20 for Keathley and Canary lineation sets, respectively. These uncertainties become greater (as

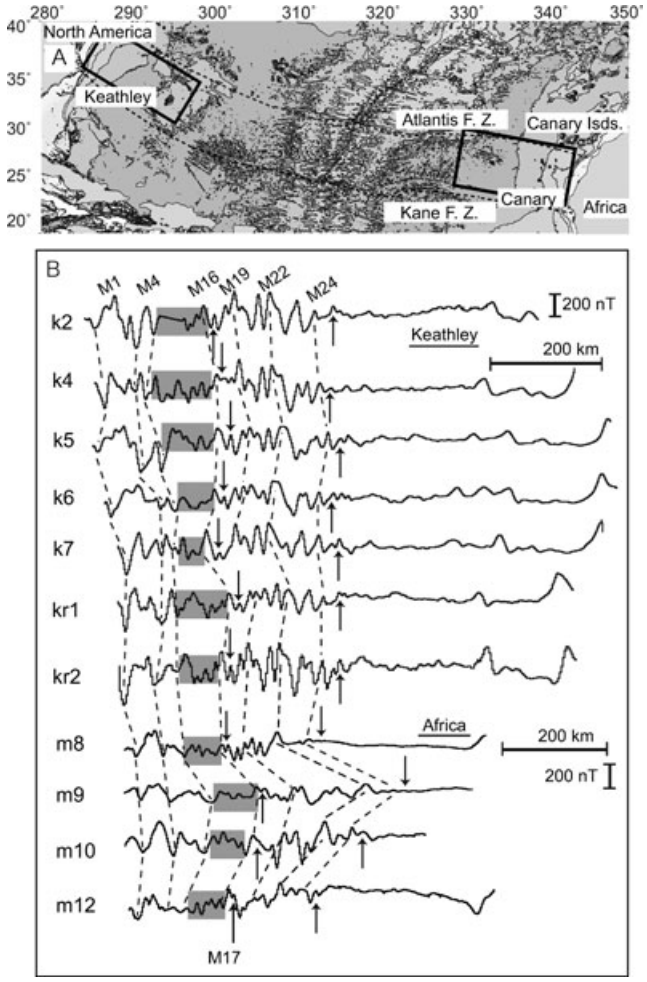

Figure 15. Summary of north Atlantic and northwest Australia M-anomalies. Part I. (A) locations of the Keathley and Canary lineation sets. Dotted lines indicate Atlantis fracture zone (north) and Kane fracture zone (south). (B) Selected anomaly profiles from the north Atlantic basin. k2–k7, kr1–kr2 and m8–m12 are profiles listed in Appendix A. Grey boxes indicate the poorly expressed anomalies in the Atlantic M5r–M15r. Dashed lines indicate anomaly correlations. Part II. (C) Northwest Australia lineation sets. A, Argo Abyssal Plain; J, Joey Rise; R, Roo Rise; G, Gascoyne Abyssal Plain and C, Cuvier Abyssal Plain. Solid and dotted lines indicate fracture zones and ridge jumps identified in Sager *et al.* (1992). (D) Selected M0–M4 anomaly profiles from the magnetic profiles shown in C. Corresponding anomalies from Pacific lineation sets are also shown. Dashed lines indicate anomaly correlations. (E) Selected M17–M25 anomaly profiles from the magnetic profiles shown in C. Dashed lines indicate anomaly correlations. Corresponding anomalies from Pacific lineation sets are also shown.

high as 36 km) through M17–M25 and M21r–M25 in the Keathley and Canary lineation sets, respectively. The increase probably results from difficulty in identifying short duration polarity blocks that characterize pre-M22 anomalies. After we calculated the locations of the polarity boundaries, the block models were averaged, resulting in Keathley and Canary average models (Fig. 16). Anomalies from M5 to M16 are not included because they are poorly expressed and difficult to correlate in the North Atlantic (Fig. 15, Appendix B, Tominaga & Sager 2010).

The Keathley and Canary block models show little difference from one another in the distribution of polarities through M16–M25, indicating the spreading system at the contemporaneous north Mid-Atlantic Ridge was nearly symmetric. In contrast, the distribution of

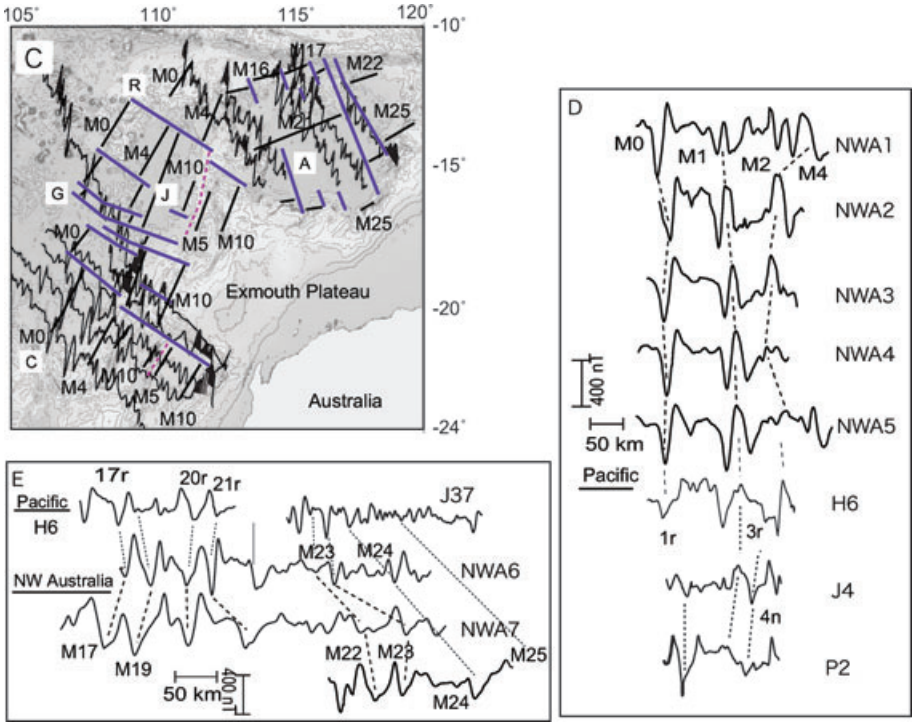

Figure 15. (*Continued*.)

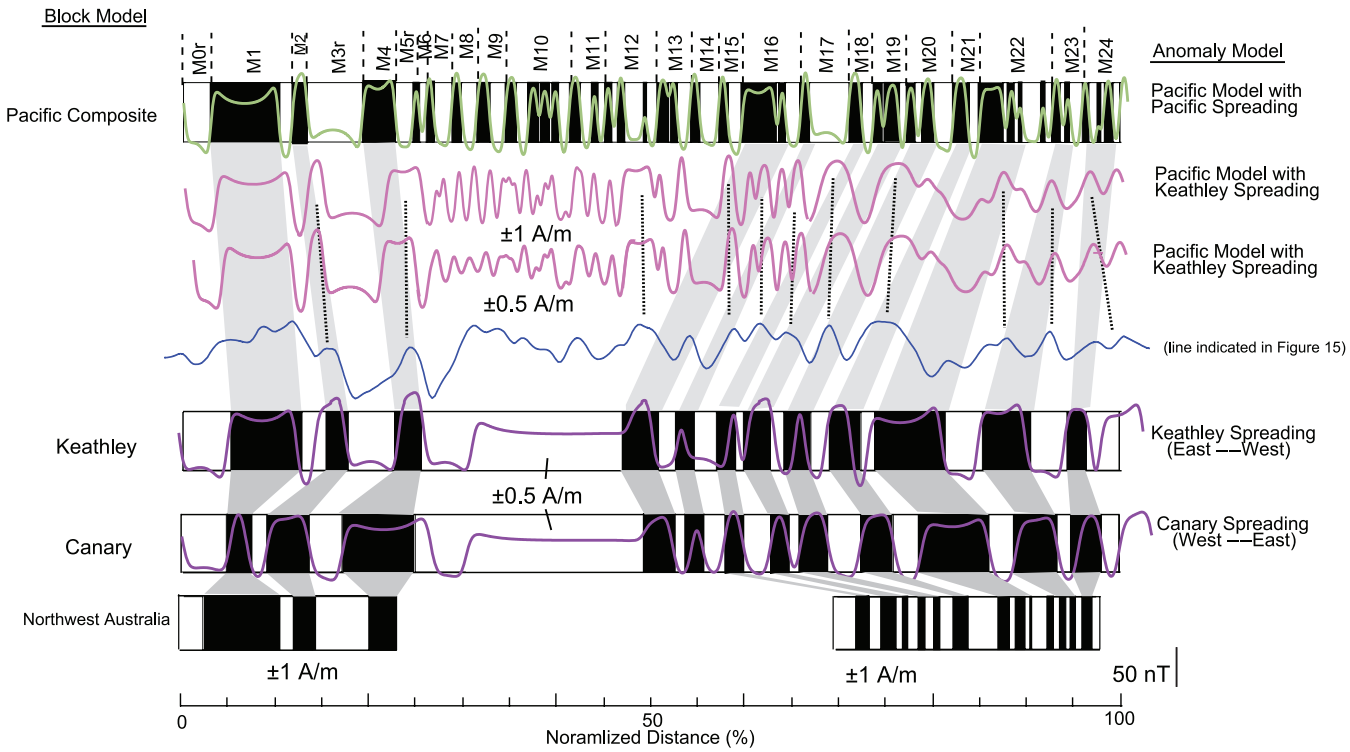

Figure 16. Polarity block models for the Keathley and Canary lineation sets in comparison to the Pacific composite model. M5r–M15r are left blank in the Keathley and Canary models because these anomalies are poorly expressed. Pale grey bands indicate correlations between the Pacific composite and Keathley, and the correlation between the Keathley and Canary lineations. Pink and green anomaly profiles are forward model results from the block models. The two pink profiles show forward model results from different magnetization values: ±1 and ±0.5 A m^{-1} (in the M5–M15 zone) for upper and lower profiles, respectively. The green anomaly profile indicates the calculated anomaly from the Pacific composite model and the pink anomaly profiles show the calculated anomaly from the Pacific composite model with its spreading rate adjusted to fit the Keathley sequence. The blue profile shows an example of observed anomalies from the Keathley anomalies (k5 in Fig. 15). The purple anomaly profiles indicate the calculated anomaly from the Keathley and Canary model.

polarities show greater differences through M0–M4, implying the spreading system was asymmetric. The asymmetric spreading in the Atlantic is thought to indicate the interaction between the MAR and a mantle plume (Müller *et al.* 1998) or ridge jumps caused by asthenospheric flow during the M0–M4 period (Bird *et al.* 2007).

4.8.2 Comparison between the pacific and atlantic GPTS models

To investigate how well the Pacific composite GPTS model represents the nature of global M-anomalies, we compared synthetic anomaly profiles calculated by forward modelling of the Pacific anomalies to the Keathley and Canary block models. We used a magnetization distribution of ± 0.5 A m^{-1} for the low amplitude M5–M15 blocks and ± 1 A m^{-1} for the rest of blocks (Fig. 16). These calculated anomaly profiles from the Pacific composite model are presented in Fig. 16. We show a synthetic anomaly profile calculated with the Pacific spreading rates and two others that are synthetic anomaly profiles calculated using the Keathley anomaly spreading rates, but with different magnetization values.

The Pacific synthetic anomaly profile with Keathley spreading rates shows good agreement to that of the Keathley model for M0–M4 anomalies and to that of the Keathley and Canary models for M16–M25 anomalies. Lesser agreement for the Canary M0–M5 anomalies apparently results from asymmetric spreading. For the M16–M25 period, the Pacific model anomalies have slightly greater amplitudes and are more distinct as compared to the Atlantic model. The Atlantic spreading system was evidently less capable of resolving the anomalies, perhaps because of slower spreading or a wider crustal accretion zone that may blur the anomalies. During the M5–M15 period, which is blank in the Atlantic model, Atlantic anomalies are greatly diminished in amplitude, to the point of being difficult to correlate. As seen in Fig. 16, the reduced magnetization Pacific anomaly model at Atlantic spreading rates shows much more distinct anomalies, implying that this diminution is not simply an effect of the spreading rate difference, but some more fundamental difference in the recording process. The discussion of this issue is beyond the scope of this study and is presented in separate paper.

4.8.3 Atlantic spreading regime

To further investigate the implications of the Atlantic M-anomalies, we assigned ages for the polarity boundaries from the Pacific composite model to the Keathley and Canary block models (Appendix B, Tominaga & Sager 2010). It is important to note that these ages for the polarity boundaries are based on the assumption of constant spreading rates and ratios in the Pacific model. Both Keathley and Canary block models show four distinctive periods of constant spreading rates: M25n–M21, M21n–M16n, M15r–M5r and M5n–M0r (Fig. 17). The divisions prior to M16 are consistent with those defined by Sundvik & Larson (1988), however, our analysis suggests M15r–M5r as one spreading phase whereas they defined the spreading change at M10N. North Atlantic spreading rates dropped at M21 by nearly a factor of two. At M16n, the spreading rate again dropped by a factor of two, with spreading at only 9.5 km Myr^{-1} for the Keathley lineations and 7.1 km Myr^{-1} for the Canary lineations. After $\sim$10 Myr of slow spreading, the spreading rates increased, approximately doubling from M5r to M0 (Fig. 17).

The shift from long-term spreading rate decline (M25–M5) to increase (M4–M0) in spreading rates coincides with changes in the variability in the distribution of polarities. Recall that the distribution of the Keathley and Canary polarity blocks show polarity

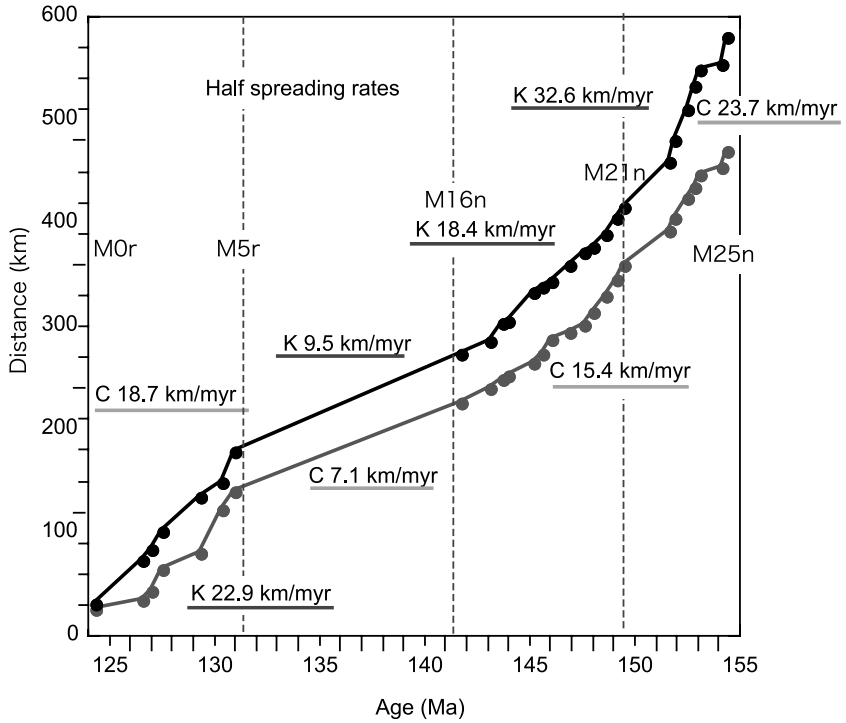

Figure 17. Half spreading rates calculated from averaged Keathley and Canary M-anomalies using the Pacific anomaly model (Appendix B). Four different periods of nearly uniform spreading rates are suggested (dashed lines). Pale grey solid circles indicate the polarity boundary in the Canary anomalies. Darker grey solid circles indicate the Keathley anomalies. K, Keathley spreading rates and C, Canary spreading rates.

spacing nearly equal during M25–M16 but are asymmetric from M4 to M0. This coincidence implies that a significant change in spreading regime occurred at the paleo Mid-Atlantic Ridge at the time of M5–M4. The nearly identical polarity distribution between Keathley and Canary models through the period of M24–M16, with intermediate-slow spreading rates, suggests that the Mid Atlantic Ridge spreading regime was similar to that of modern day intermediate spreading ridges. We assume that while the spreading rates gradually dropped from intermediate to almost ultra-slow during this time period, the symmetric spreading regime gradually shifted to asymmetric spreading as seen during the period of M4–M0.

4.8.4 Northwest Australia lineation set

To further examine the global validity of the Pacific GPTS, we also compared our timescale to the northwest Australia M-anomaly lineation set (Figs 15 C–E). The northwest Australia sequences show very similar anomaly characteristics (i.e. spacing, amplitude, shape) to that of the Pacific anomalies, probably because of the intermediate to fast spreading rates (Robb *et al.* 2005). With the northwest Australian lineation set, we are unable to construct a continuous polarity block model because the anomaly sequence is missing a large section (M7–M15) between the anomaly sequences in the Cuvier-Gascoyne and Argo abyssal plains (Fig. 15C). Furthermore, parts of the Gascoyne sequence are difficult to model owing to ridge jumps (Fullerton *et al.* 1989; Robb *et al.* 2005).

For the comparison of the Pacific and Australian M-anomalies, we focused on two piece meal sections: M0–M4 and M17–M24 (Figs 15D–E). A total of five profiles from Cuvier Abyssal plain and two profiles from Argo Abyssal plain were used to construct M0–M4 and M17–M25 block models, respectively (Fig. 16). The methodology for the construction of block models was the same as for the Keathley and Canary block models (Appendix C). Overall distribution of polarity spacing agrees with that of the Pacific, including short wavelength features in the anomalies prior to M17. The similarity between the Pacific and northwest Australia anomalies and the agreement in polarity spacing between their block models indicate that the Pacific-based GPTS provides an adequate model for the northwest Australia lineation set.

5 CONCLUSIONS

(1) We collected and correlated 87 segments of magnetic profiles covering all three Pacific M-anomaly lineation sets and constructed a revised GPTS model that spans M0 to M29. Two dates were used to calibrate the GPTS, one for M0r (125 Ma) and one for M26n (155.7 Ma), with linear interpolation in between. Although age constraint is poor, our compilation represents a wider and statistically more robust analysis of anomalies, giving a more reliable record of changes in the Earth's geomagnetic field than previous models.

(2) Overall anomaly correlations among the three lineation sets are excellent and major polarity chrons are mostly unchanged from previous studies. New subchrons were identified in M13 and M16, whereas one subchron was dropped from M11 and M24.

(3) The new M-anomaly GPTS shows minor differences in the spacing of polarity chrons as compared with previous models because (i) we used a broad selection of magnetic anomaly profiles, and (ii) a few anomaly correlations were changed, such as adding subchrons (M13 and M16) and dropping subchrons (M11 and M24). The new GPTS shows more regular spacing of polarity zones than previous GPTS because it is not focused on a small number of Hawaiian anomaly profiles.

(4) Careful selection of anomaly profiles made it possible to build a robust block model in which the accuracy of the location of polarity boundaries (average standard deviation 9–14 km) is similar to that of well accepted C-anomaly block model of Cande and Kent (1992).

(5) Interpretation and application of pre-M24 anomalies should be approached with caution because the small amplitude, short-wavelength anomalies that characterize the pre-M24 sequence are more difficult to correlate uniquely than younger anomalies.

(6) Comparison among spreading regimes in the three lineation sets indicates that all had almost the same spreading history. Two minor changes in relative spreading are observed around M13–M15 and M20–M21.

(7) The good agreement between the Pacific, Atlantic and northwest Australian anomalies implies that the Pacific model is representative of the global anomaly signal.

ACKNOWLEDGMENTS

The authors thank Jim Ogg for his encouragement and constructive comments on this work. This work was supported by the Jane & R. Ken Williams'45 Chair of Ocean Drilling Science and Technology. Data used in this study were obtained through the National Geophysical Data Center, a branch of the National Oceanographic and Atmospheric Administration (NOAA).

REFERENCES

Abrams, L.J., Larson, R.L., Shipley, T.H. & Lancelot, Y., 1992. The seismic stratigraphy and sedimentary history of the east mariana and Pigafetta Basins of the western Pacific, *Proc. ODP, Sci. Res.,* **129,** 551–569.

Besse, J. & Courtillot, V., 2002. Apparent and true polar wander and the geometry of the geomagnetic field over the last 200 Myr, *J. geophys. Res.,* **107,** doi:10.1029/2000JB000050.

Bird, D.E., Hall, S.A., Burke, K., Casey, J.F. & Sawyer, D.S., 2007. Early Central Atlantic Ocean seafloor spreading history, *Geosphere,* **3,** 283–298.

Bowles, J., Tauxe, L., Gee, J., McMillan, D. & Cande, S., 2003. Source of tiny wiggles in Chron C5: a comparison of seimentary relative intensity and marine magnetic anoamlies, *Geochem. Geophys. Geosys.,* **4,** doi:10.1029/2002GC000489.

Cande, S.C. & Kent, D.V., 1976. Constraints imposed by the shape of marine magnetic anomalies on the magnetic source, *J. geophys. Res.,* **81,** 4157–4162.

Cande, S.C. & Kent, D.V., 1992a. A new geomagnetic polarity time scale for the Late Cretaceous and Cenozoic, *J. geophys. Res.,* **97,** 13 917–13 951.

Cande, S.C. & Kent, D.V., 1992b. Ultrahigh resolution marine magnetic anomaly profiles—a record of continuous paleointensity variations? *J. geophys. Res.,* **97,** 15 075–15 083.

Cande, S.C., Larson, R.L. & Labrecque, J.L., 1978. Magnetic lineations in the Pacific Jurassic quiet zone, *Earth planet. Sci. Lett.,* **41,** 434–440.

Chambers, L.M., Pringle, M.S. & Fitton, J.G., 2004. Phreatomagmatic eruptions on the Ontong Java Plateau: an Aptian Ar/Ar age for volcaniclastic rockes at ODP Site 1184, *Origin and Evolution of the Ontong Java Plateau,* pp. 325–331, eds Fitton, J.G., Mahoney, J.J., Wallace, P.J. & Saunders, A.D., Geological Society, London, Special Publications.

Channell, J.E.T., Erba, E., Nakanishi, M. & Tamaki, K., 1995. Late Jurassic-Early Cretaceous time scales and oceanic magnetic anomaly block models, in *Geochronology, Time Scales, and Global Stratigraphic Correlation,* SEPM Special Publication No. 54, pp. 51–63, eds Berggren W.A., *et al.,* Society of Economic Mineralogy and Petrology, Tulsa, OK.

Channell, J.E.T., Erba, E., Muttoni, G. & Tremolada, F., 2000. Early Cretaceous magnetic stratigraphy in the APTICORE drill core and adjacent outcrop at Cismon (Southern Alps, Italy), and correlation to the

proposed Barremian-Aptian boundary stratotype, *Geol. Soc. Amer. Bull.,* **112,** 1430–1443.

Cooper, A.K., Marlow, M.S. & Scholl, D.W., 1976. Mesozoic magnetic lineations in the Bering Sea marginal basin, *J. geophys. Res.,* **81,** 1916–1934.

Dyment, J., Cande, S.C. & Arkani-Hamed, J., 1994. Skewness of marine magnetic anomalies created between 85 and 40 Ma in the Indian Ocean, *J. geophys. Res.,* **99,** 24 121–24 134.

Fiet, N., Quidelleur, X., Parize, O., Bulot, L.G. & Gillot, P.Y., 2006. Lower Cretaceous stage duration scombining radiometric data and orbital chronology: towards a more stable relative time scale? *Earth planet. Sci. Lett.,* **246,** 407–417.

Fullerton, L.G., Sager, W.W. & Handschumacher, D.W., 1989. Late Jurassic-Early Cretaceous evolution of the eastern Indian ocean adjacent to northwest Australia, *J. geophys. Res.,* **94,** 2937–2953.

Gaina, G., Müller, R.D., Brown, B., Ishihara, T. & Ivanov, S., 2007. Breakup and early seafloor spreading between India and Antarctica, *Geophys. J. Int.,* **170,** 151–169.

Gong, Z., Langereis, C.G. & Mullender, T.A.T., 2008. The rotation of Iberia during the Aptian and the opening of the Bay of Biscay, *Earth planet. Sci. Lett.,* **273,** 80–93.

Gladczenko, T.P., Hinz, K., Eldholm, O., Meyer, H., Neben, S. & Skogseid, J., 1997. South Atlantic volcanic margins, *J. geol. Soc. Lond.,* **154,** 465–470.

Gradstein, F.M., Agterberg, F.P., Ogg, J.G., Hardenbol, J., Van Veen, P., Thierry, J. & Huang, Z., 1995. A Triassic, Jurassic and Cretaceous time scale, in *Geochronology, Time Scales and Global Stratigraphic Correlations,* SEPM Spec. Pub. No. 54, pp. 95–126, eds Berggren W.A., *et al.,* Society of Economic Mineralogy and Petrology, Tulsa, OK.

Gradstein, F.M., Ogg, J.G. & Smith, A.G., 2005. *A Geological Time Scale 2004,* 589pp., Cambridge University Press, Cambridge.

Gubbins, D., 2004. *Time Series Analysis and Inverse Theory for Geophysicists,* 272pp., Cambridge University Press, Cambridge.

Gurevich, N.I., Merkur'ev, S.A. & Sbel'skaya, A.A., 2006. Evolution of the southern part of the Canada Basin (Arctic Ocean) based on magnetometric data, *Doklady Earth Sciences (Doklady Akademii Nauk),* **407,** 308–311.

Handshumacher, D.W., Sager, W.W., Hilde, T.W.C. & Bracey, D.R., 1988. Pre-Cretaceous tectonic evolution of the Pacific Plate and extension of the geomagnetic polarity reversal time scale with implications for the origin of the Jurassic Quiet Zone, *Tectonophysics,* **155,** 365–380.

Harland, W.B., Cox, A.V., Llewellyn, P.G., Pickton, C.A.G., Smith, A.G. & Walters, R., 1982. *A Geologic Time Scale,* 131pp., Cambridge University Press, Cambridge.

Harland, W.B., Armstrong, R.L., Cox, A.V., Craig, L.E., Smith, A.G. & Smith, D.G., 1989. *A Geologic Time Scale,* 279pp., Cambridge University Press, Cambridge.

Hayes, D.E. & Rabinowitz, P.D., 1975. Mesozoic magnetic lineations and the magnetic quiet zone off Northwest Africa, *Earth planet. Sci. Lett.,* **28,** 105–115.

He, H., Pan, Y., Tauxe, L. & Quin, R., 2008. Toward age determination of the M0r (Barremian-Aptian boundary) of the Early Cretaceous, *Phys. Earth. planet. Inter.,* **169,** 41–48.

Heirtzler, J.R., Dickson, G.O., Herron, E.M., Pitman, W.C., III & Pichon, X., 1968. Marine magnetic anomalies, geomagnetic field reversals, and motions of the ocean floor, *J. geophys. Res.,* **73,** 2119–2136.

Huang, C., Hinnov, L.A., Fischer, A.G. & Grippo, A., 2009. Astronomical tuning of the Aptian Stage (Piobbico core, Italy), *AAPG Annual Convention,* Abstract.

Klitgord, K.D. & Schouten, H., 1986. Plate kinematics of the central Atlantic, in *The Geology of North America, Volume M., The Western North Atlantic Region,* pp. 351–378, eds Vogt, P.R. & Tucholke, B.E., Geological Society of America, Boulder, CO.

Koppers, A.P., Staudigel, H. & Duncan, R.A., 2003. High-resolution ^{40}Ar/^{39}Ar dating of the oldest oceanic basement basalts in the western Pacific basin, *Geochem. Geophys. Geosyst.,* doi.10.1029/2003GC000574.

Larson, R.L. & Pitman, W.C., III, 1972. World-wide correlation of Mesozoic magnetic anomalies, and its implications, *Geol. Soc. Amer. Bull.,* **83,** 3645–3661.

Larson, R.L., 1975. Late Jurassic sea floor spreading in the eastern Indian Ocean, *Geology,* **3,** 69–71.

Larson, R.L., 1977. Early Cretaceous breakup of Gondwanaland off western Australia, *Geology,* **5,** 57–60.

Larson, R.L. & Hilde, T.W.C., 1975. A revised time scale of magnetic reversals for the Early Cretaceous and late Jurassic, *J. geophys. Res.,* **80,** 2586–2594.

Larson, R.L. & Sager, W.W., 1992. Skewness of magnetic anomalies M0 to M29 in the northwestern Pacific, *Proc. ODP Sci. Res.,* **129,** 471–481.

Lawver, L.A., Sclater, J.G. & Meinke, L., 1985. Mesozoic and Cenozoic reconstructions of the South Atlantic, *Tectonophysics,* **114,** 233–254.

Ludden, J.N., 1992. Radiometric age determinations for basement from Sites 765 and 766, Argo Abyssal Plain and northwestern Australian margin, *Proc. ODP. Sci. Res.,* **123,** 557–559.

Milner, S.C., Le Roex, A.P. & O'Connor, J.M., 1995. Age of Mesozoic igneous rocks in northwestern Namibia, and their relationship to continental breakup, *J. geol. Soc., Lond.,* **152,** 97–104.

Müller, D., Roest, W.R. & Royer, J.-Y., 1998. Asymmetric sea-floor spreading caused by ridge plume interactions, *Nature,* **396,** 455–459.

Nakanishi, M., Tamaki, K. & Kobayashi, K., 1989. Mesozoic magnetic anomaly lineations and seafloor spreading history of the northwestern Pacific, *J. geophys. Res.,* **94,** 15 437–15 462.

Nakanishi, M., Tamaki, K. & Kobayashi, K., 1992. Magnetic anomaly lineations from late Jurassic to Early Cretaceous in the west-central Pacific Ocean, *Geophys. J. Int.,* **109,** 701–719.

Nakanishi, M., Sager, W.W. & Klaus., A., 1999. Magnetic lineations within Shatsky Rise, northwest Pacific Ocean: Implications for hot spot-triple junction interaction and oceanic plateau formation, *J. geophys. Res.,* **104,** 7539–7556.

Ogg, J.G. & Gutowski, J., 1995. Oxfordian Magnetic Polarity Time Scale, in *Proceedings of the 4th International Congress on Jurassic Stratigraphy and Geology, Geo. Res. Forum vols. 1–2,* pp. 406–414, ed. Riccardi, A.C., Trabs-Tec Publication Ltd., Zurich, Switzerland.

Pálfy, J., Smith, P.L. & Mortensen, J.K., 2000. A U-Pb and ^{40}Ar/^{39}Ar time scale for the Jurassic, *Can. J. Earth Sci.,* **37,** 923–944.

Parker, R.L. & Huestis, S.P., 1974. The inversion of magnetic anomalies in the presence of topography, *J. geophys. Res.,* **79,** 1587–1593.

Petronotis, K.E., Gordon, R.G. & Acton, G.D., 1992. Determining paleomagnetic poles and anomalous skewness from marine magnetic anomaly skewness data from a single plate, *Geophys. J. Int.,* **109,** 209–224.

Plessis, A.D. & Simpson, E.S.W., 1974. Magnetic anomalies associated with the southeastern continental margin of south Africa, *Marine geophys. Res.,* **2,** 99–110.

Pringle, M., Chambers, L. & Ogg, J.M., 2003. synchronicity of volcanism on Ontong Java and Manihiki Plateau with global oceanographic events?, EGS-AGU-EUG Joint Assembly, Abstract #13768.

Przybylski, P.A. & Ogg, J.M., 2007. Calibration of pre-M25 marine magnetic anomalies: magnetic polarity composite of Late Callovian through Kimmerdigdian, *EOS Trans. AGU,* **88**(52), Fall. Meet. Supp., Abstract T13A-1130.

Rabinowitz, P.D. & LaBrecque, J., 1979. The Mesozoic South Atlantic Ocean and evolution of its continental margins, *J. geophys. Res.,* **84,** 5973–6002.

Rabinowitz, P.D., Coffin, M.F. & Falvey, D., 1983. The separation of Madagascar and Africa, *Science,* **220,** 67–69.

Ramana, M.V., Nair, R.R., Sarma, K.V.L.N.S., *et al*. 1994. Mesozoic anomalies in the Bay of Bengal, *Earth planet. Sci. Lett.,* **121,** 469–475.

Ramana, M.V., Ramprasad, T. & Desa, M., 2001. Seafloor spreading magnetic anomalies in the Enderby Basin, East Antarctica, *Earth. planet. Sci. Lett.,* **191,** 241–255.

Robb, M.S., Taylor, B. & Goodlife, A.M., 2005. Re-examination of the magnetic linations of the Gascoyne and Cuvier Abyssal Plains, off NW Australia, *Geophys. J. Int.,* **163,** 42–55.

Roest, W.R., Danobeitia, J.J., Verhoef, J. & Collette, B.J., 1992. Magnetic anomalies in the Canary basin and the mesozoic evolution of the central north Atlantic, *Mar. geophys. Res.,* **14,** 1–24.

Roeser, H.A., Steiner, C., Schreckenberger, B. & Block, M., 2002. Structural development of the Jurassic Magnetic Quuiet Zone off Morocco and identification of Middle Jurassic magnetic linations, *J. geophys. Res.,* **107,** doi:10.1029/2000JB000094.

Rybakov, M., Goldshmidt, V., Fleischer, L. & Ben-Gai, Y., 2000. 3-D gravity and magnetic interpretation for the Hifa Bay area (Israel), *J. appl. Geophys.,* **44,** 353–367.

Sager, W.W., Fullerton, L.G., Buffler, R.T. & Handschumacher, D.W., 1992. Argo Abyssal Plain magnetic lineations revisited: implications for the onset of seafloor spreading and tectonic evolution of the eastern Indian ocean, *Proc. ODP. Sci. Res.,* **123,** 659–669.

Sager, W.W., Weiss, C.J., Tivey, M.A. & Johnson, H.P., 1998. Geomagnetic polarity reversal model of deep-tow profiles from the Pacific Jurassic Quiet Zone, *J. geophys. Res.,* **103,** 5269–5286.

Schouten, H. & McCamy, K., 1972. Filtering marine magnetic anomalies, *J. geophys. Res.,* **77,** 7089–7099.

Selby, D., Mutterlose, J. & Condon, D.J., 2009. U-Pb and Re-Os geochronology of the Aptian/Albian and Cenomanian/Turonian stage boundaries: implications for time scale calibration, osmium isotope seawater composition and Re-Os systematics in organic-rich sediments, *Chem. Geol.,* **265,** 394–409, doi:10.1016/j.chemgeo.2009.1005.1005.

Schouten, H. & Cande, S.C., 1976. Paleomagnetic Poles from marine magnetic anomalies, *J. geophys. Res.,* **44,** 567–575.

Schouten, H. & Klitgord, K.D., 1982. The memory of the accreting plate boundary and the continuity of fracture zones, *Earth planet. Sci. Lett.,* **59,** 255–266.

Sibuet, J.-C., Srivastava, S.P. & Spakman, W., 2004. Pyrenean ogogeny and plate kinematics, *J. geophys. Res.,* **109,** doi:10.1029/2003JB002514.

Srivastava, S.P., Sibuet, J.-C., Cande, S., Roest, W.R. & Reid, I.D., 2000. Magnetic evidence for slow seafloor spreading during the formation of the Newfoundland and Iberian margins, *Earth planet. Sci. Lett.,* **182,** 61–76.

Speranza, F., Satolli, S., Mattioli, E. & Calamita, F., 2005. Magnetic stratigraphy of Kimmeridgian-Aptian sections from Umbria-Marche (Italy): new details on the M polarity sequence, *J. geophys. Res.,* **110,** doi:10.1029/2005JB003884.

Sundvik, M.T. & Larson, R.L., 1988. Seafloor spreading history of the western North Atlantic basin derived from the Keathley sequence and computer graphics, *Tectonophysics,* **155,** 49–71.

Tivey, M.A., Sager, W.W., Lee, S.-M. & Tominaga, M., 2006. Origin of the Pacific Jurassic Quiet Zone, *Geology,* **34,** 789–792.

Tominaga, M. & Sager, W.W., 2010. The Tectonic origin of the magnetic smooth zone in early cretaceous North Atlantic, *Geophys. Res. Lett.,* **37,** doi:10.1029/2009GL040984.

Tominaga, M., Sager, W.W., Tivey, M.A. & Lee, S.-M., 2008. Deep-tow magnetic anomaly study of the Pacific Jurassic Quiet Zone and implications for the geomagnetic polarity reversal time scale and geomagnetic field behavior, *J. geophys. Res.,* **113,** doi:10.1029/2007JB005527.

Verhoef, J. & Scholten, R.D., 1983. Cross-over analysis of marine magnetic anomalies, *Marine geophys. Res.,* **5,** 421–435.

Vine, F.J. & Matthews, D.H., 1963. Magnetic anomalies over oceanic ridges, *Nature,* **199,** 47–949.

Vogt, P.R., Anderson, C.N. & Bracey, D.R., 1971a. Mesozoic magnetic anomalies, sea-floor spreading, and geomagnetic reversals in the southwestern North Atlantic, *J. geophys. Res.,* **76,** 4796–4923.

Vogt, P.R., Johnson, G.L., Holcombe, T.L., Gilg, J.G. & Avery, O.E., 1971b. Episodes of sea-floor spreading recorded by the North Atlantic basement, *Tectonophysics,* **12,** 211–234.

Whitmarsh, R.B., Dean, S.M., Minshull, T.A. & Topkins, M., 2000. Tectonic implications for exposure of lower continental crust beneath the Iberia Abyssal Plain, Northeast Atlantic Ocean: Geophysical evidence, *Tectonics,* **19,** 919–942.

APPENDIX A: ATLANTIC MAGNETIC PROFILES AND MAGNETIZATION PARAMETERS

NGDC#	Cruise ID	Anomaly	Index	Site lat	Site lon	Pole lat	Pole lon	PI	PD	Slin
Keathley lineations										
09100001	Keathley	M2	k2	32.7	297.0	71.9	193.5	45.3	−19.8	190
		M5	k2	32.7	295.0	69.5	193.5	44.9	−22.6	190
		M15	k2	32.7	293.0	71.0	181.0	41.7	−19.3	190
		M22	k2	32.7	290.0	73.7	158.7	37.8	−13.1	190
		M2	k4	33.0	297.0	71.9	193.5	45.7	−19.9	190
		M5	k4	33.0	295.0	69.5	193.5	45.3	−22.7	190
		M15	k4	33.0	293.0	71.0	181.0	42.1	−19.4	190
		M22	k4	33.0	290.0	73.7	158.7	38.3	−13.1	190
		M2	k5	33.3	297.0	71.9	193.5	46.1	−20.0	190
		M5	k5	33.3	295.0	69.5	193.5	45.7	−22.7	190
		M15	k5	33.3	293.0	71.0	181.0	42.5	−19.4	190
		M22	k5	33.3	290.0	73.7	158.7	38.7	−13.2	190
		M2	k6	34.0	297.0	71.9	193.5	46.9	−20.1	190
		M5	k6	34.0	295.0	69.5	193.5	46.4	−22.9	190
		M15	k6	34.0	293.0	71.0	181.0	43.4	−19.5	190
		M22	k6	34.0	290.0	73.7	158.7	39.6	−13.2	190
		M2	k7	33.7	297.0	71.9	193.5	46.5	−20.0	190
		M5	k7	33.7	295.0	69.5	193.5	46.1	−22.8	190
		M15	k7	33.7	293.0	71.0	181.0	42.9	−19.5	190
		M22	k7	33.7	290.0	73.7	158.7	39.2	−13.2	190
03030005TAG71		M2	kr1	33.0	297.0	71.9	193.5	45.7	−19.9	190
		M5	kr1	33.2	295.0	69.5	193.5	45.6	−22.7	190
		M15	kr1	33.4	293.0	71.0	181.0	42.7	−19.5	190
		M22	kr1	34.0	290.0	73.7	158.7	39.6	−13.2	190
03030015TAG70		M2	kr2	32.7	297.0	71.9	193.5	45.3	−19.8	190
		M5	kr2	32.9	295.0	69.5	193.5	45.2	−22.6	190
		M15	kr2	33.0	293.0	71.0	181.0	42.1	−19.4	190
		M22	kr2	33.7	290.0	73.7	158.7	39.2	−13.2	190
Canary lineations										
3030005	TAG71	M2	m9	22.0	332.0	52.0	261.6	48.1	−41.6	10
		M5	m9	21.5	335.0	47.9	263.3	46.6	−46.1	10
		M15	m9	21.0	337.0	49.3	262.6	44.0	−44.2	10
		M22	m9	20.5	340.0	54.0	260.3	39.5	−38.7	10
		M2	m10	23.0	332.0	52.0	261.6	49.0	−42.0	10
		M5	m10	22.5	335.0	47.9	263.3	47.5	−46.5	10
		M15	m10	22.0	337.0	49.3	262.6	44.9	−44.6	10
		M2	m12	24.0	332.0	52.0	261.6	49.8	−42.4	10
		M5	m12	23.5	335.0	47.9	263.3	48.3	−46.9	10
		M15	m12	23.0	337.0	49.3	262.6	45.8	−44.9	10
		M22	m12	22.5	340.0	54.0	260.3	41.6	−39.3	10
3030015	TAG70	M2	m8	21.5	332.0	52.0	261.6	47.7	−41.4	10
		M5	m8	21.0	335.0	47.9	263.3	46.2	−45.9	10
		M15	m8	20.5	337.0	49.3	262.6	43.5	−44.1	10
		M22	m8	20.0	340.0	54.0	260.3	39.0	−38.6	10

NGDC#, NGDC archive number; ID, survey ID in NGDC archive; anomaly, a chron number in which approximately an anomaly profile starts; index, profile ID indicated on Figure 15; site lat, latitude of a middle point on a given magnetic profile segment; site lon, longitude of a middle point on a given magnetic profile segment; pole lat, paleo pole latitude; pole lon, paleo pole longitude; PI, paleo inclination of a given profile; PD, paleo declination of a given profile; slin, track line azimuth from north towards young direction of the lienation.

APPENDIX B: STANDARD DEVIATIONS OF ATLANTIC POLARITY MODEL CHRON BOUNDARIES (IN KILOMETRE)

Chron	Age	Canary	std (km)	*n*	Block (per cent)	Keathley	Std (km)	*n*	Block (per cent)
M0r	124.14	0.00	0.00	4	0.00	0.00	0.00	7	0.00
M1n	125.00	23.27	4.99	3	4.98	28.80	4.48	5	4.99
M1r	127.15	30.87	6.20	3	6.60	70.38	14.77	5	12.19
M3n	127.57	40.55	7.78	4	8.67	80.90	9.65	4	14.01
M3r	128.05	60.95	6.26	4	13.04	99.19	16.24	7	17.18
M4	129.80	77.10	9.72	4	16.49	131.30	17.79	5	22.74
M5r	130.84	119.77	15.54	3	25.62	146.30	9.79	4	25.33
void	131.42	136.75	23.47	4	29.25	175.38	13.76	5	30.37
M16n	141.83	222.83	8.09	4	47.66	269.86	17.85	5	46.73
M16r	143.20	236.23	8.17	4	50.53	283.18	18.95	4	49.03
M17n	143.72	245.93	7.73	3	52.60	299.54	23.37	5	51.87
M17r	143.97	250.05	9.63	4	53.48	301.75	22.03	4	52.25
M18n	145.21	261.10	6.58	4	55.85	329.48	20.35	4	57.05
M18r	145.61	269.73	14.68	4	57.69	334.72	24.18	5	57.96
M19n	146.00	283.58	11.61	4	60.65	339.84	24.38	5	58.85
M19r	146.82	291.88	14.57	4	62.43	356.52	26.42	5	61.74
M20n	147.50	297.68	13.16	4	63.67	369.18	28.07	4	63.93
M20r	147.90	310.98	13.00	4	66.51	374.15	24.84	4	64.79
M21n	148.54	326.53	16.33	4	69.84	386.68	25.74	4	66.96
M21r	148.98	342.78	34.61	4	73.32	402.40	27.86	4	69.68
M22n	149.37	356.00	36.42	4	76.14	411.90	27.57	4	71.32
M22r	151.44	388.68	42.46	4	83.13	456.37	25.75	3	79.02
M23n	151.68	401.70	36.36	4	85.92	477.98	25.94	5	82.77
M23r	152.24	421.68	33.50	4	90.19	506.36	31.54	5	87.68
M24n	152.61	431.73	33.78	3	92.34	529.74	28.99	5	91.73
M24r	152.83	443.38	33.17	4	94.83	546.43	32.76	4	94.62
M25n	153.81	451.40	34.16	4	96.55	551.15	24.69	4	95.44
M25r	154.08	467.53	28.80	4	100.00	577.50	26.26	5	100.00

Chron, chron identified in the north Atlantic M-anomalies; age, ages of the polarity boundaries determined from the Pacific compilation block model; Canary, averaged locations of polarity boundaries in Canary lineation set in km; std (km), standard deviation of the locations of polarity boundaries in km; n, number of profiles used to calculate the average and standard deviation; block (per cent), normalized distance at each polarity boundary from M0r; Keathley, averaged locations of polarity boundaries in Keathley lination set in km.

APPENDIX C: MAGNETIC PROFILES AND MAGNETIZATION PARAMETERS (NORTHWEST AUSTRALIA)

NGDC#	Cruise ID	Anomaly	Index	Site lat	Site lon	Pole lat	Pole lon	PI	PD	Slin
23060036	ODP123	M0	NWA1	−15.0	108.0	51.7	330.3	−59.4	−33.1	190
01030204	V3308	M0	NWA2	−19.0	108.5	51.7	330.3	−62.5	−34.9	190
		M0	NWA3	−20.0	108	51.7	330.3	−62.9	−35.9	190
		M0	NWA4	−21.0	107.5	51.7	330.3	−63.3	−36.5	190
01030201	V3305	M0	NWA5	−22.0	107	51.7	330.3	−65.8	−37.3	190
02020079	A2093	M17	NWA6	−13.0	116.5	47.7	342.8	−57.6	−38.3	190
		M17	NWA7	−14.0	115.5	47.7	342.8	−57.8	−39.2	190

NGDC#, NGDC archive number; ID, survey ID in NGDC archive; anomaly, a chron number in which approximately an anomaly profile starts; index, profile ID indicated on Figure 15; site lat, latitude of a middle point on a given magnetic profile segment; site lon, longitude of a middle point on a given magnetic profile segment; pole lat, paleo pole latitude; pole lon, paleo pole longitude; PI, paleo inclination of a given profile; PD, paleo declination of a given profile; slin, track line azimuth from north towards young direction of the lienation.